

Maximally Symmetric Boost-Invariant Solutions of the Boltzmann Equation in Foliated Geometries

Mauricio Martinez,^a Christopher Plumberg^b

^a*Department of Chemistry and Biochemistry, 103 Chemistry and Biochemistry Building, Bozeman, 59717, MT, USA*

^b*Natural Science Division, Pepperdine University, Malibu, CA 90263, USA*

ABSTRACT: In this work we study the relativistic kinetic theory of a boost-invariant conformal gas on a static, maximally symmetric background $dS_3 \times \mathbb{R}$, considering all constant-curvature slicings of dS_3 - flat, spherical, or hyperbolic- and their associated symmetry groups. Using a symmetry-driven cotangent-bundle approach, we show that the isometry group of each slicing acts on phase space in such a way that only its Casimir invariants and the time-like coordinate unconstrained, so the distribution function depends solely on these quantities. This yields a unified boost-invariant exact solution of the Boltzmann equation valid for each constant-curvature foliation of $dS_3 \times \mathbb{R}$. Specializing this general solution to the flat and spherical foliations reproduces the Bjorken and Gubser flows, respectively, while its restriction to the hyperbolic foliation produces a genuinely new analytic solution ('Grozdanov flow'). Hydrodynamics and free streaming emerge naturally as limiting regimes of this novel exact solution. We further comment on several relevant aspects of the new boost-invariant solution on the hyperbolic slicing and on their interpretation once mapped back to Minkowski space.

Contents

1	Introduction	2
2	Cotangent bundle formulation of kinetic theory	3
2.1	Symmetry Constraints on the Distribution Function	5
3	Boltzmann equation and its general solution on foliated $dS_3 \times \mathbb{R}$	8
3.1	From Minkowski $\mathbb{R}^{3,1}$ to foliated $dS_3 \times \mathbb{R}$	8
3.2	Isometries of $dS_3 \times \mathbb{R}$ foliations	9
3.3	Symmetry Constraints on the Distribution Function in Foliated $dS_3 \times \mathbb{R}$	11
3.4	Casimirs of the foliated $dS_3 \times \mathbb{R}$ geometry	12
3.4.1	Casimir of the 2d constant curvature foliation Σ_κ	12
3.4.2	Casimir for E_1	14
3.5	Reduced Boltzmann equation in a $dS_3 \times \mathbb{R}$ foliation	14
4	From exact kinetics to macroscopic dynamics in $dS_3 \times \mathbb{R}$ slicings	15
4.1	Energy–momentum tensor from the exact solution on foliated $dS_3 \times \mathbb{R}$ geometry	15
4.1.1	Landau matching conditions	16
4.2	Emergent Hydrodynamics in foliated $dS_3 \times \mathbb{R}$	16
4.2.1	Ideal hydrodynamics	16
4.2.2	Viscous hydrodynamics	17
4.2.3	Navier-Stokes limit	18
4.2.4	Second-order conformal hydrodynamics	18
4.3	Free streaming in $dS_3 \times \mathbb{R}$ slices	21
5	From foliated $dS_3 \times \mathbb{R}$ to Minkowski $\mathbb{R}^{3,1}$	21
5.1	Interpreting Slice-depending Casimirs in Minkowski Space	22
5.1.1	Momentum transformation and radial–boost structure	22
5.1.2	Casimirs in terms of boosted momenta	25
6	Conclusions	25
A	Killing vectors of a 2d constant curvature manifold	26
A.1	Lie algebra	28
B	Anisotropic integrals	29
C	The approximate cold-limit solution	30

1 Introduction

The study of linear and nonlinear equations of motion lies at the foundation of modern theoretical and computational physics. Such equations provide the essential framework for describing, modeling, and simulating complex dynamical phenomena across a wide range of scales. In particular, nonlinear transport processes are commonly approached through kinetic theory, where the Boltzmann equation plays a central role as the microscopic description underlying the emergent macroscopic evolution.

The Boltzmann equation is an inherently high-dimensional integro-PDE governing the seven-dimensional on-shell one-particle distribution function, and its solutions typically require computationally intensive numerical methods. Exact analytical solutions are exceptionally rare, yet they provide powerful insight into nonlinear and far-from-equilibrium physics. The limited number of known solutions, both in non-relativistic [1–3] and relativistic [4–13] settings, arise only under special circumstances, such as high degrees of symmetry or simplified collision kernels. Beyond their theoretical importance, exact solutions of the Boltzmann equation provide indispensable benchmarks for testing, validating, and calibrating sophisticated Boltzmann transport algorithms, see Ref. [14].

Recently, Grozdanov introduced an elegant construction of both inviscid and viscous boost-invariant hydrodynamic solutions arising from a *hyperbolic slicing* of $dS_3 \times \mathbb{R}$, hereafter referred to as the ‘Grozdanov flow’. Building on the geometric method of Gubser and Yarom [15], his analysis clarifies that the Bjorken [16] and Gubser [17] flows are not related by a generalisation of the former, but instead belong - together with his new boost invariant solution - to a unified family of three maximally symmetric boost-invariant conformal flows. These correspond respectively to the flat $ISO(2)$, spherical $SO(3)$ and hyperbolic $SO(2, 1)$ foliations of the same auxiliary $dS_3 \times \mathbb{R}$ geometry¹. From this novel viewpoint, the Grozdanov flow is on equal conceptual footing with Bjorken and Gubser: all three are coordinate projections of a single geometric construction, each preserving a three-dimensional non-Abelian isometry group.

Motivated by the geometric insights underlying the Grozdanov flow, we develop in this work the kinetic theory of an uncharged conformal relativistic gas evolving on a maximally symmetric $dS_3 \times \mathbb{R}$ background. Adopting Grozdanov’s unifying perspective, we formulate the microscopic description of the Bjorken [16], Gubser [17], and Grozdanov [18] flows within a single kinetic-theory framework. Our results follow from applying the cotangent-bundle formulation of relativistic kinetic theory [19–24], which makes transparent the role of symmetry generators and Casimir invariants in determining the structure and dynamics of an expanding gas on any foliation of $dS_3 \times \mathbb{R}$ and in reducing the complexity of the Boltzmann equation. Solving the Boltzmann equation directly in this unified geometry allows us to recover the known kinetic solutions for Bjorken [13] and Gubser flows [4, 5] and, crucially, to obtain a new exact solution describing a gas undergoing Grozdanov flow. This unified viewpoint also clarifies how distinct macroscopic behaviors—hydrodynamical and non-hydrodynamic free streaming regimes—emerge from the same microscopic description in different dynamical limits.

¹In Gubser’s original formulation [17], the symmetry group is denoted as $SO_q(3)$. Here we omit the subscript q , while keeping in mind that this notation refers to the same underlying flow solution.

We have organized the paper as follows. Section 2 introduces the cotangent-bundle formulation of kinetic theory and explains how symmetry choices constrain the distribution function. Section 3 applies this framework to the Boltzmann equation on foliated $dS_3 \times \mathbb{R}$ geometries, deriving the corresponding symmetry generators, Casimirs, reduced kinetic equation, and exact solutions for each foliation. Section 4 analyzes the macroscopic dynamics emerging from these solutions, including ideal, viscous, and second-order hydrodynamics, as well as free streaming. Section 5 highlights key features of the $dS_3 \times \mathbb{R}$ solutions when mapped back to Minkowski space. Conclusions are presented in Section 6, with technical details provided in the appendices.

Before proceeding, we clarify our notation. A hat (the symbol ‘^’) written above a variable or tensor denotes that the corresponding quantity is defined in $dS_3 \times \mathbb{R}$ or dS_3 space. To distinguish scalars, tensors, and other entities corresponding to different foliations of dS_3 , we use the label κ (or (κ)) as a subscript or superscript². The metric signature follows the ‘mostly plus’ convention.

2 Cotangent bundle formulation of kinetic theory

In this section, we briefly review the cotangent bundle formulation of relativistic kinetic theory on a generic curved manifold. Beyond its elegant geometric structure, this formulation offers a transparent way to understand how symmetries constrain the functional form of the distribution function. A comprehensive discussion of this formalism can be found in Refs. [19–21]. An alternative, albeit equivalent, description formulated for the tangent bundle can be found in Refs. [22–24] and references therein. The reader primarily interested in the symmetry constraints of the distribution function in $dS_3 \times \mathbb{R}$ may proceed directly to Sect. 3.4.

Relativistic kinetic theory [25, 26] in a curved spacetime can be naturally formulated on the cotangent bundle $\mathcal{T}^*\mathcal{M}$ of the spacetime manifold \mathcal{M} [19, 20, 27, 28]. Within this formulation, each point of $\mathcal{T}^*\mathcal{M}$ represents a spacetime event $x^\mu \in \mathcal{M}$ together with a co-vector p_μ at this event. p_μ represents the canonical momentum of the particle at x^μ .³ The one-particle distribution function $f(x^\mu, p_i)$ is thus defined as a non-negative function of the seven-dimensional on-shell mass submanifold of $\mathcal{T}^*\mathcal{M}$,

$$\Gamma = \{(x^\mu, p_i) : x^\mu \in \mathcal{M}, p_i \in \mathcal{T}_x^*\mathcal{M} | g_{\mu\nu} p^\mu p^\nu = 0, p^0 > 0\}; \quad (2.1)$$

In other words, Γ is the massless on-shell submanifold of the cotangent bundle ($\mathcal{T}^*\mathcal{M}$) with positive timelike momentum component p^0 and thus constitutes the full 7-dimensional relativistic phase space.

In this picture, the evolution of the system is governed by the Liouville vector field \mathcal{L} ,

$$\mathcal{L} = p^\mu \frac{\partial}{\partial x^\mu} + \Gamma_{\mu i}^\lambda p_\lambda p^\mu \frac{\partial}{\partial p_i}, \quad (2.2)$$

which generates the free-streaming flow in phase space and is tangent to $\mathcal{T}^*\mathcal{M}$. In the presence of collisions among particle constituents, the relativistic Boltzmann equation can be written compactly

²The choice is purely notational and context-dependent. For example, writing $\hat{A}_i^{(\kappa)}$ emphasizes that \hat{A}_i is a vector associated with the κ foliation (rather than a component of a second-rank tensor), whereas using d_κ (or $d^{(\kappa)}$) simply indicates that the scalar d on that particular foliation.

³The zeroth component of the momentum is determined via the on-shell massless condition, i.e., $p_0 = p_0(g_{\mu\nu}, x^\mu, p_i)$.

as

$$\mathcal{L}[f] = C[f], \quad \Rightarrow \quad p^\mu \partial_\mu f + \Gamma_{\mu i}^\lambda p_\lambda p^\mu \frac{\partial f}{\partial p_i} = C[f], \quad (2.3)$$

where $C[f]$ is the collisional kernel. In this work we model the collisional kernel $C[f]$ to be given by the relaxation time approximation (RTA) [29, 30]

$$C[f] = \frac{p \cdot u}{\tau_r} [f(x^\mu, p_i) - f_{eq.}(x^\mu, p_i, T)]. \quad (2.4)$$

In the previous expression T is the temperature in the local rest frame, u^μ is the fluid velocity, τ_r is the relaxation time scale and $f_{eq.}$ is the Jüttner thermal equilibrium distribution function. The fluid velocity is chosen to be defined in the Landau frame. In addition, Weyl invariance demands that the relaxation time be inversely proportional to the temperature so $\tau_r = \gamma/T$. For the relaxation time approximation (2.4) the proportionality constant is related to the shear viscosity over entropy ratio as follows

$$\gamma = 5 \frac{\eta}{S} \Rightarrow \tau_r = 5 \frac{\eta}{S} \frac{1}{T}. \quad (2.5)$$

Although the previous derivation is obtained from first principles [31], in numerical studies of the RTA Boltzmann equation [4, 5, 32, 33], it is common to regard η/S as a tunable parameter, enabling one to explore the crossover from nearly ideal to strongly viscous dynamics. In this setting, the relation (2.5) is often rewritten as $\tau_r = c \eta / (ST)$ with η/S taken as a fixed input and c regarded as an adjustable constant. In this work we follow this convention. For a given solution of the Boltzmann equation, it is possible to determine macroscopic physical observables by considering the moments of the distribution function. For instance, the energy momentum tensor reads as

$$T^{\mu\nu} = \langle p^\mu p^\nu \rangle, \quad (2.6)$$

where we denote the momentum moment of an arbitrary physical observable $\mathcal{O}(x^\mu, p_i)$ as $\langle \mathcal{O}(x^\mu, p_i) \rangle_X = \int_p \mathcal{O}(x^\mu, p_i) f_X(x^\mu, p_i)$ being the momentum measure $\int_p \equiv \int d^3 p / [(2\pi)^3 p^0]$. The energy density ϵ , pressure \mathcal{P} and shear-stress tensor $\pi^{\mu\nu}$ are read from the previous expression by splitting the momentum into its spatial and temporal components, i.e., $p^\mu = -(u \cdot p)u^\mu + p^{(\mu}$ with $p^{(\mu)} = \Delta^{\mu\nu} p_\nu$ where $\Delta^{\mu\nu} = g^{\mu\nu} + u^\mu u^\nu$ is a projector orthogonal to the fluid velocity u^μ . By using this decomposition of the particle's momentum, the energy-momentum tensor (2.6) is written as

$$T^{\mu\nu} = \epsilon(x^\mu) u^\mu u^\nu + \Delta^{\mu\nu}(x^\mu) \mathcal{P}(x^\mu) + \pi^{\mu\nu}(x^\mu), \quad (2.7)$$

where

$$\epsilon(x^\mu) = \langle (-u \cdot p)^2 \rangle, \quad (2.8a)$$

$$\mathcal{P}(x^\mu) = \frac{1}{3} \langle \Delta_{\mu\nu} p^\nu p^\mu \rangle, \quad (2.8b)$$

$$\pi^{\mu\nu}(x^\mu) = \langle p^{(\mu} p^{\nu)} \rangle. \quad (2.8c)$$

In Eq. (2.8c) we use the shorthand notation $p^{(\mu} p^{\nu)} = \Delta_{\alpha\beta}^{\mu\nu} p^\alpha p^\beta$, where the projector

$$\Delta_{\alpha\beta}^{\mu\nu} = \frac{1}{2} \left(\Delta_\alpha^\mu \Delta_\beta^\nu + \Delta_\beta^\mu \Delta_\alpha^\nu - \frac{2}{3} \Delta^{\mu\nu} \Delta_{\alpha\beta} \right),$$

extracts the traceless, u^μ -orthogonal component of a rank-2 tensor.

2.1 Symmetry Constraints on the Distribution Function

A spacetime symmetry generated by a Killing vector field \mathcal{K} of \mathcal{M} induces a canonical lift to the cotangent bundle $\mathcal{T}^* \mathcal{M}$, that is, a natural extension of \mathcal{K} from spacetime to phase space, which acts not only on the spacetime coordinates but also on the momentum components in a way that preserves the canonical symplectic structure. In adapted local coordinates,⁴ the canonical lift of a spacetime Killing vector field \mathcal{K} to the cotangent bundle takes the form [19–21]

$$\tilde{\mathcal{K}} = \mathcal{K}^\mu \frac{\partial}{\partial x^\mu} - p_\alpha \frac{\partial \mathcal{K}^\alpha}{\partial x^\mu} \frac{\partial}{\partial p_\mu}, \quad (2.9)$$

which acts on the distribution function as a directional derivative in phase space. It is possible to rewrite the previous expression as follows

$$\tilde{\mathcal{K}} = \mathcal{K}^\mu \frac{D}{\partial x^\mu} - p_\alpha (\nabla_\nu \mathcal{K}^\alpha) \frac{\partial}{\partial p_\nu}. \quad (2.10)$$

The operators appearing in (2.10) decompose the geometry of the cotangent bundle into *horizontal* and *vertical* directions. The horizontal basis vector

$$\frac{D}{\partial x^\mu} = \frac{\partial}{\partial x^\mu} + \Gamma_{\mu\nu}^\alpha p_\alpha \frac{\partial}{\partial p_\nu}, \quad (2.11)$$

represents infinitesimal displacements in spacetime that are *lifted* to phase space so that momenta are parallel transported along the underlying connection. In contrast, vertical basis vectors $\partial/\partial p_\mu$ generate pure variations in momentum at fixed spacetime position. Together, $\{D/\partial x^\mu, \partial/\partial p_\nu\}$ provide a covariant splitting of the tangent space of the cotangent bundle, $T(T^*M) = H(T^*M) \oplus V(T^*M)$, into horizontal (spacetime) and vertical (momentum) directions. Finally, the covariant derivative of the Killing vector field \mathcal{K}^λ in Eq. (2.10) is given by

$$\nabla_\nu \mathcal{K}^\lambda = \partial_\nu \mathcal{K}^\lambda + \Gamma_{\nu\sigma}^\lambda \mathcal{K}^\sigma, \quad (2.12)$$

so that the second term in the RHS of Eq. (2.10) accounts for the induced change in momentum caused by the variation of \mathcal{K} along the connection. This construction ensures that $\hat{\mathcal{K}}$ acts intrinsically on phase-space functions without reference to any coordinate-dependent artifact. Now, the

⁴By *adapted local coordinates* we refer to the coordinates (x^μ, p_μ) which provide at each point $(x, p) \in \mathcal{T}^* \mathcal{M}$ a basis of vector fields $\{\partial_{x^\mu}|_{(x,p)}, \partial_{p_\mu}|_{(x,p)}\}$ and associated dual basis of covector fields $\{dx^\mu|_{(x,p)}, dp_\mu|_{(x,p)}\}$ [21]. Hence, any vector field V in $\mathcal{T}^* \mathcal{M}$ can be expanded locally as

$$V = X^\mu \frac{\partial}{\partial x^\mu} + Y_\mu \frac{\partial}{\partial p_\mu}, \quad X^\mu = dx^\mu(V), \quad Y_\mu = dp_\mu(V).$$

associated momentum map,

$$\mathcal{J}_{\mathcal{K}} = p_{\mu} \mathcal{K}^{\mu}, \quad (2.13)$$

remains constant along particle trajectories. In other words, $\mathcal{J}_{\mathcal{K}}$ is conserved along the geodesic Liouville flow when \mathcal{K} is a Killing vector field, since the Liouville operator acts on $\mathcal{J}_{\mathcal{K}}$ as $\mathcal{L}[\mathcal{J}_{\mathcal{K}}] = 0$. A distribution function is said to *share the symmetry* generated by \mathcal{K} when it is invariant under the lifted flow, that is,

$$\mathcal{L}_{\widehat{\mathcal{K}}} f = 0. \quad (2.14)$$

where \mathcal{L}_X refers to the Lie derivative with respect to the vector field X . Equation (2.14) expresses that f is constant along the integral curves of $\widehat{\mathcal{K}}$ and depends only on the invariants of the symmetry group. In practice, the condition of invariance of the distribution function (2.14) along the flow generated by a Killing vector reduces to a first-order linear PDE⁵

$$\mathcal{K}^{\mu} \frac{\partial f}{\partial x^{\mu}} - p_{\alpha} \frac{\partial \mathcal{K}^{\alpha}}{\partial x^{\mu}} \frac{\partial f}{\partial p_{\mu}} = 0. \quad (2.15)$$

This equation can be interpreted as the vanishing of the total derivative of f along the flow generated by $\widehat{\mathcal{K}}$ in phase space. By introducing an affine parameter λ along integral curves of this vector field, we impose

$$\frac{df}{d\lambda} = \frac{dx^{\mu}}{d\lambda} \frac{\partial f}{\partial x^{\mu}} + \frac{dp^{\mu}}{d\lambda} \frac{\partial f}{\partial p_{\mu}} = 0, \quad (2.16)$$

where we identify the characteristic equations

$$\frac{dx^{\mu}}{d\lambda} = \mathcal{K}^{\mu}, \quad (2.17a)$$

$$\frac{dp^{\mu}}{d\lambda} = -p_{\alpha} \frac{\partial \mathcal{K}^{\alpha}}{\partial x^{\mu}}. \quad (2.17b)$$

The integrals of this system yield the momentum–map invariants $\mathcal{J}_{\mathcal{K}}$ (2.13), associated with the Killing vector field \mathcal{K} . Now, in the case when we have a set of Killing vectors \mathcal{K}_a ($a = 1, \dots, N$) forming a Lie algebra, the corresponding conditions $\mathcal{L}_{\widehat{\mathcal{K}}_a} f = 0$ define a system of first–order characteristic equations in phase space. In the adapted local coordinates (x^{μ}, p_{ν}) on $\mathcal{T}^*\mathcal{M}$, the invariants obtained from the characteristic system of the lifted Killing fields coincide with the momentum maps associated with each symmetry generator, $\mathcal{J}_a = p_{\mu} \mathcal{K}_a^{\mu}$. Under the Poisson bracket, the momentum maps satisfy the same Lie–algebra relations as the Killing vectors from which they are constructed. Now, by differentiating \mathcal{J}_a along the lifted flow, i.e., along a given trajectory, yields

$$\frac{d\mathcal{J}_a}{d\lambda} = p_{\mu} \frac{d\mathcal{K}_a^{\mu}}{d\lambda} + \mathcal{K}_a^{\mu} \frac{dp_{\mu}}{d\lambda} = 0, \quad (2.18)$$

where we make use of Eq. (2.17b). This expression shows that the quantities derived through the characteristic equations in adapted local coordinates are precisely these momentum maps expressed in that basis. Hence, the general solution of $\mathcal{L}_{\widehat{\mathcal{K}}_a} f = 0$ can locally be written as a function of the

⁵The distribution function $f = f(x^{\mu}, p_i)$ is defined in the mass shell section of the total phase space γ_m (2.1), so p_0 is constrained by the on-mass shell condition. The lifted Killing vector $\widehat{\mathcal{K}}$ is tangent to γ_m since $\widehat{\mathcal{K}}(g_{\mu\nu} p^{\mu} p^{\nu}) = 0$ for any Killing vector field. Hence, the invariance condition (2.14) remains valid when f is restricted to be on-shell variables.

corresponding momentum maps,

$$f(x^\mu, p_i) = f(\mathcal{J}_1(x^\mu, p_i), \mathcal{J}_2(x^\mu, p_i), \dots, \mathcal{J}_N(x^\mu, p_i)). \quad (2.19)$$

This expression reflects the fact that symmetry considerations restrict the distribution function to depend only on the corresponding momentum maps. The characteristic equations identify the phase-space directions along which the distribution function is constant, but they do not determine which combinations of variables are globally invariant under the full symmetry group. In other words, Eq. (2.19) indicates that the distribution function remains constant along the phase-space trajectories generated by the infinitesimal symmetries of the system. However, this local invariance does not imply full invariance under the finite action of the symmetry group. The set $\{\mathcal{J}_a\}$ transforms among itself under the coadjoint representation of the group⁶, so only particular combinations of them - the Casimir invariants of the algebra - remain globally invariant under the full group action.

A natural question within the cotangent bundle formalism is whether this symmetry reduction extends to the collision term, and to what extent the symmetries of the distribution function constrain the functional structure of the collisional kernel. The answer is now well understood [21]: invariance of the distribution function alone, Eqs. (2.14) and (2.19), does not restrict the collision kernel. Rather, the decisive requirement is the invariance of the microscopic transition rate under the complete lift of the same symmetry group. If the transition probability $\mathcal{W}(x^\mu, p \rightarrow p')$ entering in the collisional kernel satisfies

$$\mathcal{L}_{\tilde{\mathcal{K}}_a} \mathcal{W}(x^\mu, p \rightarrow p') = 0 \quad \forall \tilde{\mathcal{K}}_a, \quad (2.20)$$

then the collision operator $C[f]$ is form-invariant under the lifted symmetry and maps symmetric distributions to symmetric distributions. This result was established rigorously by Acuña et al. [21] (see Appendix F therein): *symmetry constraints on the collision term arise only from the lifted invariance of the transition rate, not from imposing $\mathcal{L}_{\tilde{\mathcal{K}}_a} f = 0$ by itself*. For the RTA collision kernel (2.4) used in this work, this model is automatically compatible with the isometry generators associated to each $dS_3 \times \mathbb{R}$ slicing, as shown in Sect. 3.3.

We conclude by noting that when both symmetry conditions are satisfied - namely the invariance of the distribution function under the lifted generators, Eqs. (2.14), and the invariance of the transition amplitude, Eq. (2.20) - the full Boltzmann equation consistently reduces to a symmetry-protected evolution equation for the distribution function. In this case, the physically relevant solutions depend only on the Casimir invariants of the symmetry group,

$$f(x^\mu, p_i) = f(C_1(\{\mathcal{J}_a\}), C_2(\{\mathcal{J}_a\}), \dots), \quad (2.21)$$

which guaranties full invariance under the action of the symmetry group.

⁶The coadjoint representation describes how a symmetry group acts on its own conserved quantities, while the Casimirs are the combinations of those quantities that remain invariant under any such action. Geometrically, this means that while the momentum maps label individual orbits of the coadjoint action, the Casimirs are the quantities that remain constant across each orbit, defining the invariant geometry of the phase-space manifold. For example, when the rotation group $SO(3)$, acts on space, it rotates the components of the angular momentum, changing their direction but not their magnitude. That invariant magnitude—the length of the angular momentum vector—is precisely the Casimir of $SO(3)$.

3 Boltzmann equation and its general solution on foliated $dS_3 \times \mathbb{R}$

In this section, we apply the cotangent bundle formalism to derive an exact solution of the Boltzmann equation corresponding to a chosen foliation of $dS_3 \times \mathbb{R}$. We start by reviewing the key features of $dS_3 \times \mathbb{R}$ and its possible foliations.

3.1 From Minkowski $\mathbb{R}^{3,1}$ to foliated $dS_3 \times \mathbb{R}$

The line element in Minkowski space coordinates is

$$ds^2 = -dt^2 + dx^2 + dy^2 + dz^2 \quad (3.1)$$

For systems undergoing boost-invariant evolution, a more natural choice is the Milne coordinates

$$\tau = \sqrt{t^2 - z^2}, \quad \zeta = \frac{1}{2} \ln \left| \frac{t+z}{t-z} \right|, \quad (3.2)$$

for which

$$ds^2 = -d\tau^2 + dx^2 + dy^2 + \tau^2 d\zeta^2 = -d\tau^2 + dr^2 + rd\phi^2 + \tau^2 d\zeta^2 \quad (3.3)$$

To map this into $dS_3 \times \mathbb{R}$, we first note that de Sitter space dS_3 (with unit radius) can be embedded in $\mathbb{R}^{3,1}$ as the hyperboloid defined by

$$-(X^0)^2 + \sum_{m=1}^3 (X^m)^2 = 1, \quad (3.4)$$

and may be parameterized by the coordinates

$$X^0 = -\frac{1 - q^2(\tau^2 - r^2)}{2q\tau}, \quad X^i = \frac{x^i}{\tau}, \quad X^3 = \frac{1 + q^2(\tau^2 - r^2)}{2qr}, \quad (3.5)$$

where $q > 0$ is an arbitrary parameter. The line element of dS_3 is then expressible as

$$d\hat{s}^2 = \frac{1}{\tau^2} (-d\tau^2 + dx^2 + dy^2) \quad (3.6)$$

As shown in [18], one can distinguish three different ways to foliate the hyperboloid which preserve the maximum degree of symmetry: foliations at constant X^0 , constant $X^3 - X^0$, and constant X^3 . Each leaf of a given foliation intersects the hyperboloid along a 2d (boost-invariant) surface with constant curvature κ , corresponding to flat ($\kappa = 0$), spherical ($\kappa = +1$) and hyperbolic ($\kappa = -1$) foliations. One parameterizes a given foliation by defining a time-like coordinate ρ and a space-like coordinate θ , such that ρ indexes the leaf of the foliation and θ parametrizes the leaf itself.

If one foliates by $X^0 \equiv \sinh \rho$ and takes the remaining coordinates to be proportional to a unit vector $X^m = \cosh \rho r^m$ as done in [15], one finds from Eq. (3.4) that the metric (3.6) becomes

$$d\hat{s}^2 = -d\rho^2 + \cosh^2 \rho (d\theta^2 + \sin^2 \theta d\phi^2) \quad (3.7)$$

On the other hand, one may foliate by $X^3 = \cosh \rho$ and take the remaining coordinates to be proportional to a unit vector in a lower dimensional de Sitter space:

$$d\hat{s}^2 = -d\rho^2 + \sinh^2 \rho (d\theta^2 + \sinh^2 \theta d\phi^2) \quad (3.8)$$

The first foliation therefore corresponds to leaves with uniform positive (spherical) curvature and the second to leaves with uniform negative (hyperbolic) curvature. The third type of foliation by $X^3 - X^0 = \frac{1}{q^\tau} \equiv \frac{1}{q} e^{-\rho}$ yields a uniform space with zero (flat) curvature with metric

$$d\hat{s}^2 = -d\rho^2 + e^{-2\rho} (d\theta^2 + \theta^2 d\phi^2), \quad (3.9)$$

which corresponds to a spatially flat 2d universe undergoing Hubble *contraction* with a scale factor given by $a(\rho) = e^{-\rho}$ and θ playing the role of a radial coordinate.

We can rewrite Eqs. (3.7)-(3.9) in a more compact notation by introducing

$$d\Sigma_\kappa^2 \equiv \begin{cases} d\theta^2 + \sin^2 \theta d\phi^2 & \kappa = +1 \\ d\theta^2 + \theta^2 d\phi^2 & \kappa = 0 \\ d\theta^2 + \sinh^2 \theta d\phi^2 & \kappa = -1 \end{cases} \quad (3.10)$$

With this notation, we can parametrize the infinitesimal interval between two events in any foliation of $dS_3 \times \mathbb{R}$ by

$$\begin{aligned} d\hat{s}_\kappa^2 &= \hat{g}_{\mu\nu} d\hat{x}^\mu d\hat{x}^\nu = -d\rho^2 + S_\kappa^2(\rho) d\Sigma_\kappa^2 + d\zeta^2, \\ &= -d\rho^2 + S_\kappa^2(\rho) (d\theta^2 + Q_\kappa^2(\theta) d\phi^2) + d\zeta^2, \end{aligned} \quad (3.11)$$

where the subindex κ labels the specific foliation of $dS_3 \times \mathbb{R}$ as defined above [18]. Here the set of coordinates (ρ, θ, ϕ) parametrize dS_3 while $\zeta \in (-\infty, \infty)$ parametrizes \mathbb{R} , and the functions $S_\kappa(\rho)$ and $Q_\kappa(\theta)$ as well as the associated coordinate ranges for each foliation are listed in Table 1. Below, we denote a single leaf in the κ foliation by $\Sigma_\kappa \subset dS_3$. A concise summary of the geometrical structure of 2d surfaces with constant curvature, their Killing vector fields and their Lie algebra is provided in App. A.

Table 1: Definitions of $S_\kappa(\rho)$ and $Q_\kappa(\theta)$, together with the corresponding coordinate ranges for different spatial curvatures according to Ref. [18].

κ	$S_\kappa(\rho)$	$Q_\kappa(\theta)$	ρ range	θ range	ϕ range
0	$e^{-\rho}$	θ	$-\infty < \rho < \infty$	$0 \leq \theta < \infty$	$0 \leq \phi < 2\pi$
+1	$\cosh \rho$	$\sin \theta$	$-\infty < \rho < \infty$	$0 \leq \theta < 2\pi$	$0 \leq \phi < 2\pi$
-1	$\sinh \rho$	$\sinh \theta$	$0 < \rho < \infty$	$0 \leq \theta < \infty$	$0 \leq \phi < 2\pi$

3.2 Isometries of $dS_3 \times \mathbb{R}$ foliations

The full isometry group of the spacetime $\mathcal{M} = dS_3 \times \mathbb{R}$ is $SO(3, 1) \times E_1$ where $SO(3, 1)$ group acts on the de Sitter coordinates, while the one-dimensional euclidean group E_1 acts along the ad-

ditional ζ . The latter can be written as $E_1 = T_1 \rtimes O(1)$ where T_1 denotes the one-dimensional translation group, and $O(1)$ is the one-dimensional orthogonal group consisting of the identity and reflection through the origin. Hence, $O(1)$ encodes both orientation-preserving and orientation-reversing isometries of the line, and is isomorphic to the discrete group \mathbb{Z}_2 , i.e. $O(1) \cong \mathbb{Z}_2$. The de Sitter space dS_3 can be foliated into 2d slices that preserve the maximum amount of symmetries [18]. Therefore, each leaf of a foliation defines a specific spatial geometry whose associated isometries determine the invariants under the full action of the isometry group.

The Killing vectors of the constant curvature slice Σ_κ of dS_3 are ⁷

$$\hat{\mathcal{K}}_1^{(\kappa)}(\theta, \phi, \kappa) = \cos \phi \partial_\theta - G_\kappa(\theta) \sin \phi \partial_\phi, \quad (3.12a)$$

$$\hat{\mathcal{K}}_2^{(\kappa)}(\theta, \phi, \kappa) = \sin \phi \partial_\theta + G_\kappa(\theta) \cos \phi \partial_\phi, \quad (3.12b)$$

$$\hat{\mathcal{K}}_3^{(\kappa)}(\theta, \phi, \kappa) = \partial_\phi, \quad (3.12c)$$

$$\hat{\mathcal{K}}_\zeta = \partial_\zeta, \quad (3.12d)$$

where $G_\kappa(\theta) = Q'_\kappa(\theta)/Q_\kappa(\theta)$, see App. A for details. The first three terms in this expression correspond to the Killing vectors generating the isometries in the slice Σ_κ , while the last term represents the Killing vector associated with the one-dimensional Euclidean subgroup E_1 . The Lie algebra of the Killing vectors (3.12) is

$$[\hat{\mathcal{K}}_A^{(\kappa)}, \hat{\mathcal{K}}_\zeta^{(\kappa)}] = 0, \quad (3.13a)$$

$$[\hat{\mathcal{K}}_A^{(\kappa)}, \hat{\mathcal{K}}_B^{(\kappa)}] = f_{AB}{}^C \hat{\mathcal{K}}_C^{(\kappa)}, \quad (3.13b)$$

with $A, B, C = 1, 2, 3$ and the structure constants $\{f_{12}{}^3, f_{23}{}^1, f_{31}{}^2\} = \{-\kappa, -1, -1\}$ (see App. A for details).

The explicit form of the three Killing vector fields $\hat{\mathcal{K}}_A^{(\kappa)}$ (3.12a)-(3.12c) and their respective algebra (3.13b) illustrates how the geometry of each foliation determines the structure of the symmetry flows:

- **For $\kappa = +1$:** The functions $G_{+1}(\theta) = \cot \theta$ and $Q_{+1}(\theta) = \sin \theta$ correspond to the metric of the two-sphere \mathbb{S}^2 . The Killing vectors $\hat{\mathcal{K}}_A^{(+1)}$ generate the $\mathfrak{so}(3)$ algebra of rotations; geometrically, they represent infinitesimal rotations around three orthogonal axes. The associated orbits are closed curves (great circles), reflecting the compact nature of the spherical foliation.
- **For $\kappa = 0$:** Here $G_0(\theta) = 1/\theta$ and $Q_0(\theta) = \theta$, corresponding to the flat metric of the Euclidean plane \mathbb{R}^2 . The Killing vectors $\hat{\mathcal{K}}_1^{(0)}$ and $\hat{\mathcal{K}}_2^{(0)}$ generate translations along orthogonal Cartesian directions, while $\hat{\mathcal{K}}_3^{(0)}$ generates planar rotations. Together, they form the Lie algebra $\mathfrak{iso}(2)$, representing the Euclidean group of motions in the plane.

⁷The one-dimensional space \mathbb{R} admits a single continuous isometry generated by the Killing vector ∂_ζ corresponding to translations along ζ . In one dimension, the Killing equation admits no other nontrivial smooth solutions; the only additional isometry is the discrete reflection $\zeta \rightarrow -\zeta$, which is not connected to the identity and therefore not generated by a Killing vector.

- **For $\kappa = -1$:** The functions $G_{-1}(\theta) = \coth \theta$ and $Q_{-1}(\theta) = \sinh \theta$ describe the metric of the hyperbolic plane \mathbb{H}^2 . The Killing vectors $\hat{\mathcal{K}}_A^{(-1)}$ generate the Lorentzian algebra $\mathfrak{so}(2, 1)$, which acts transitively on \mathbb{H}^2 . In this case, $\hat{\mathcal{K}}_3^{(-1)}$ corresponds to rotations around the symmetry axis, while $\hat{\mathcal{K}}_1^{(-1)}$ and $\hat{\mathcal{K}}_2^{(-1)}$ generate hyperbolic “boost-like” transformations that move points along geodesics of constant negative curvature.

3.3 Symmetry Constraints on the Distribution Function in Foliated $dS_3 \times \mathbb{R}$

We start this section by examining the dynamical evolution along a chosen foliation leaf Σ_κ of dS_3 . While the full de Sitter space admits the six-dimensional isometry group $SO(3, 1)$, each foliation into two-dimensional slices with constant curvature κ preserves only a three-dimensional subgroup, $\mathfrak{h}_\kappa \in \{SO(3), ISO(2), SO(2, 1)\}$ whose Killing vectors correspond to Eqs.(3.12a)-(3.12c) for a given κ . Invariance under the lifted action of \mathfrak{h}_κ restricts the distribution function to depend solely on the associated Casimir invariants, leaving its variation along the orthogonal coordinate ρ unconstrained. Hence, the evolution along ρ captures the residual dynamics after the full $SO(3, 1)$ symmetry is reduced to \mathfrak{h}_κ . This reduction reflects the geometric restriction that connects global de Sitter equilibrium to the boost-invariant flows of Bjorken [16], Gubser [15, 17] and Grozdanov [18]: once a preferred foliation is chosen, ρ becomes the genuine dynamical variable governing the evolution. Mathematically, this corresponds to a contraction of the characteristic system of first-order PDEs on the cotangent bundle $\mathcal{T}^*\mathcal{M}$: the six $SO(3, 1)$ generators defining the invariant flow reduce to the three Killing vector fields of \mathfrak{h}_κ , leaving ρ as the single non-trivial characteristic direction along which f evolves. In this sense, selecting a foliation singles out ρ as the natural dynamical parameter of the reduced geometry, capturing the physical evolution that survives the symmetry reduction. One important consequence of the fact that all isometry generators of the foliated $dS_3 \times \mathbb{R}$ leave the time-like coordinate ρ invariant is that the relaxation-time approximation automatically respects these symmetries. Since the relaxation time depends only on this invariant variable, $\tau_r \equiv \tau_r(\rho) = \gamma/\hat{T}_\kappa(\rho)$ with γ being a constant, the RTA collision term remains form-invariant under the full isometry group of the foliation.

For an exact or approximate boost-invariant solution of the Boltzmann equation, the distribution function is constrained by the lifted action of the symmetry generators of the chosen foliation Σ_κ of dS_3 that leave the constant-curvature slices $\kappa = 0, \pm 1$ invariant, together with the E_1 generator along \mathbb{R} . The number of independent variables on which the distribution function depends is directly derived from general group-theoretical arguments as follows. For a given Lie algebra \mathfrak{g} , the number of algebraically independent Casimir invariants N_C is determined by the dimension of the algebra and the rank of the antisymmetric structure matrix F_{ab} constructed from the structure constants [34, 35], namely $N_C = \dim(\mathfrak{g}) - \text{rank}(F_{ab})$. For the subalgebras associated with the constant-curvature foliations of dS_3 , $\mathfrak{h}_\kappa \in \{\mathfrak{so}(3), \mathfrak{iso}(2), \mathfrak{so}(2, 1)\}$, the structure matrix has generic rank two, yielding a single independent Casimir, $N_{\hat{C}^{(\kappa)}} = 1$. Similarly, for the one-dimensional Euclidean group $E_1 = T(1) \rtimes O(1)$, the Lie algebra $\mathfrak{e}_1 \cong \mathbb{R}$ admits one invariant, $N_{\hat{C}_\zeta} = 1$. Hence, an exact solution of the Boltzmann equation in $dS_3 \times \mathbb{R}$ that is invariant under the full isometry group action on a foliation leaf Σ_κ depends only on three independent variables: the time-like coordinate ρ , the Casimir $\hat{C}^{(\kappa)}$ associated to the isometry group of Σ_κ , and the Casimir \hat{C}_ζ

corresponding to the E_1 sector,

$$f = f\left(\rho, \hat{C}^{(\kappa)}(\{\hat{\mathcal{J}}_A^{(\kappa)}\}), \hat{C}_\zeta(\{\hat{\mathcal{J}}_\zeta\})\right). \quad (3.14)$$

3.4 Casimirs of the foliated $dS_3 \times \mathbb{R}$ geometry

In the following we proceed to calculate the Casimirs based on standard group theory methods [35].

3.4.1 Casimir of the 2d constant curvature foliation Σ_κ

The associated momentum maps of the slice Σ_κ are obtained from their definition (2.13) and the Killing vectors (3.12a)-(3.12c). These are given by

$$\hat{\mathcal{J}}_1^{(\kappa)} = p_\theta \cos \phi - p_\phi G_\kappa \sin \phi, \quad (3.15a)$$

$$\hat{\mathcal{J}}_2^{(\kappa)} = p_\theta \sin \phi + p_\phi G_\kappa \cos \phi, \quad (3.15b)$$

$$\hat{\mathcal{J}}_3^{(\kappa)} = p_\phi. \quad (3.15c)$$

The functions $\hat{\mathcal{J}}_A^{(\kappa)}$ are conserved quantities associated with the symmetry flows generated by the Killing vectors of the slice Σ_κ in dS_3 , i.e. the momentum maps on the cotangent bundle $T^*\Sigma_\kappa$. For $\kappa = +1$, they coincide with the components of the angular momentum on the spherical slice \mathbb{S}^2 , reflecting the rotational invariance of $\mathfrak{so}(3)$. For $\kappa = 0$, they represent the conserved linear and orbital momenta on the flat plane \mathbb{R}^2 , corresponding to translations and rotations generated by $\mathfrak{iso}(2)$. Finally, for $\kappa = -1$, they form the components of a Lorentz vector associated with $\mathfrak{so}(2, 1)$, describing the invariants of motion under hyperbolic ‘‘boost-like’’ transformations on the negatively curved slice \mathbb{H}^2 . Thus, the set $\{\hat{\mathcal{J}}_A^{(\kappa)}\}$ encapsulates, in a unified way, the conserved dynamical quantities for all foliations of dS_3 .

The associated momentum maps $\hat{\mathcal{J}}_A^{(\kappa)}$ (3.15) satisfy an identical algebra to the corresponding Killing vectors (3.13b) under Poisson brackets, namely

$$\{\hat{\mathcal{J}}_A^{(\kappa)}, \hat{\mathcal{J}}_B^{(\kappa)}\} = f_{AB}{}^C \hat{\mathcal{J}}_C^{(\kappa)}, \quad f_{12}{}^3 = -\kappa, \quad f_{23}{}^1 = f_{31}{}^2 = -1. \quad (3.16)$$

The quadratic Casimir is built from an ad-invariant symmetric bilinear form⁸ g^{ab} satisfying $f_{ad}{}^c g_{cb} + f_{bd}{}^c g_{ac} = 0$. For the above commutation relations, isotropy in the (1, 2)-plane allows $g_{ab} = \text{diag}(A, A, B)$, and the ad-invariance condition imposes $\kappa B - A = 0$, hence $B = A/\kappa$. Choosing the normalization $A = 1$ gives

$$g^{ab} = \text{diag}(1, 1, \kappa),$$

⁸Let \mathfrak{h} be a Lie algebra with generators T_a and structure constants $[T_a, T_b] = f_{ab}{}^c T_c$. A symmetric bilinear form g^{ab} on \mathfrak{h} is called ad-invariant if it is preserved under the adjoint action, i.e.

$$g([X, Y], Z) + g(Y, [X, Z]) = 0, \quad \forall X, Y, Z \in \mathfrak{h}.$$

In components, this condition is equivalent to

$$f_{ad}{}^c g_{cb} + f_{bd}{}^c g_{ac} = 0$$

If g_{ab} is ad-invariant then the quadratic element $g^{ab} T_a T_b$ commutes with all generators of \mathfrak{h} (i.e. is invariant under the adjoint action) and therefore defines a quadratic Casimir of the algebra.

and the resulting Casimir function

$$\hat{C}_\kappa = \left(\hat{\mathcal{J}}_1^{(\kappa)}\right)^2 + \left(\hat{\mathcal{J}}_2^{(\kappa)}\right)^2 + \kappa \left(\hat{\mathcal{J}}_3^{(\kappa)}\right)^2. \quad (3.17)$$

The Casimir invariant \hat{C}_κ represents the invariant squared distance of the momentum map vector $(\hat{\mathcal{J}}_1^{(\kappa)}, \hat{\mathcal{J}}_2^{(\kappa)}, \mathcal{J}_3)$ with respect to the metric of the constant-curvature slice Σ_κ . For $\kappa = +1$, it reduces to the familiar expression for the angular-momentum magnitude on the sphere, $\hat{C}_{+1} = \left(\hat{\mathcal{J}}_1^{(1)}\right)^2 + \left(\hat{\mathcal{J}}_2^{(1)}\right)^2 + \left(\hat{\mathcal{J}}_3^{(1)}\right)^2$, and is invariant under rotations of $\mathfrak{so}(3)$. For $\kappa = 0$, $\hat{C}_0 = \left(\hat{\mathcal{J}}_1^{(0)}\right)^2 + \left(\hat{\mathcal{J}}_2^{(0)}\right)^2$ gives the squared planar momentum invariant under the Euclidean group $\mathfrak{iso}(2)$. For $\kappa = -1$, the sign change in the third term reflects the Lorentzian signature of the hyperbolic metric, and $\hat{C}_{-1} = \left(\hat{\mathcal{J}}_1^{(-1)}\right)^2 + \left(\hat{\mathcal{J}}_2^{(-1)}\right)^2 - \left(\hat{\mathcal{J}}_3^{(-1)}\right)^2$ defines the invariant hyperbolic norm of the momentum vector—the analogue of the Minkowski length associated with $\mathfrak{so}(2, 1)$. Thus, the Casimir unifies the invariant ‘momentum norms’ across the three foliations, providing the conserved scalar quantity that labels the group orbits in phase space.

Substituting Eq. (3.15) into the Casimir (3.17) yields

$$\hat{C}_\kappa \equiv \hat{p}_{\Sigma_\kappa}^2 = \hat{p}_\theta^2 + (G_\kappa^2 + \kappa)\hat{p}_\phi^2 = \hat{p}_\theta^2 + \frac{\hat{p}_\phi^2}{Q_\kappa(\theta)^2}, \quad (3.18)$$

with $G_\kappa(\theta) = Q'_\kappa(\theta)/Q_\kappa(\theta)$ and we used the identity $G_\kappa^2 + \kappa = 1/Q_\kappa^2$. Replacing the function $Q_\kappa(\theta)$ for each curvature parameter (see Table 1) in the previous expression yields

$$\hat{C}_1 \equiv \hat{p}_{\Sigma_1}^2 = \hat{p}_\theta^2 + \frac{\hat{p}_\phi^2}{\sin^2 \theta} \quad (3.19a)$$

$$\hat{C}_0 \equiv \hat{p}_{\Sigma_0}^2 = \hat{p}_\theta^2 + \frac{\hat{p}_\phi^2}{\theta^2}, \quad (3.19b)$$

$$\hat{C}_{-1} \equiv \hat{p}_{\Sigma_{-1}}^2 = \hat{p}_\theta^2 + \frac{\hat{p}_\phi^2}{\sinh^2 \theta}. \quad (3.19c)$$

The first expression, $\hat{p}_{\Sigma_1}^2$, corresponds to the squared magnitude of the momentum on the two-sphere \mathbb{S}^2 , first derived in Refs. [4, 5]. The second, $\hat{p}_{\Sigma_0}^2$, represents the magnitude of the radial momentum in the transverse plane orthogonal to the longitudinal beam direction when written in polar coordinates—after identifying $\theta = r$ [18]—and was first obtained by Baym [13]. Finally, the third invariant, $\hat{p}_{\Sigma_{-1}}^2$, which is a novel result first derived in this work, measures the conserved norm of the momentum with respect to the hyperbolic metric $d\Sigma_{-1}^2 = d\theta^2 + \sinh^2 \theta d\phi^2$, and therefore defines the invariant squared distance along geodesics of constant negative curvature. In this sense, it constitutes the hyperbolic analogue of the Euclidean momentum magnitude. The physical interpretation of the Casimirs (3.19) will be revisited in Sec. 5.1, where we map them back to Minkowski space $\mathbb{R}^{3,1}$.

3.4.2 Casimir for E_1

The full isometry group of the spacetime $dS_3 \times \mathbb{R}$ includes an additional factor $E_1 = T(1) \rtimes O(1)$, whose Lie algebra $\mathfrak{e}_1 \cong \mathbb{R}$ has only one Casimir. For the connected translation subgroup $T(1)$, the Casimir is the conserved translation momentum map $\hat{\mathcal{J}}_\zeta = \hat{p}_\zeta$. Under the full E_1 action, which includes reflections, the globally invariant quantity is its even combination,

$$\hat{C}_\zeta = (\hat{\mathcal{J}}_\zeta)^2 = \hat{p}_\zeta^2. \quad (3.20)$$

As expected, this Casimir is the square of the momentum component along the ζ direction.

In summary, when considering the isometry group of a given foliation of $dS_3 \times \mathbb{R}$, the complete set of global invariants are given by the Casimirs of the foliated dS_3 , \hat{C}_κ (3.19), and the one associated to E_1 , and the quadratic invariant \hat{C}_ζ (3.20).

3.5 Reduced Boltzmann equation in a $dS_3 \times \mathbb{R}$ foliation

Based on the analysis carried out in the previous section, the isometry group of a foliated $dS_3 \times \mathbb{R}$ demands that

$$f^{(\kappa)}(x^\mu, p_i) = f^{(\kappa)}(\rho, \hat{p}_{\Sigma_\kappa}^2, \hat{p}_\zeta^2), \quad (3.21)$$

where $p_{\Sigma_\kappa}^2$ is given by Eq. (3.18). Because the distribution function depends exclusively on the symmetry invariants of the foliated $dS_3 \times \mathbb{R}$ geometry, its derivatives with respect to all coordinates—except ρ —and along the momentum directions vanish. The curvature effects of the foliated dS_3 are fully encoded in the invariant momentum combinations $\hat{p}_{\Sigma_\kappa}^2$, yielding a single effective Boltzmann equation along ρ . Thus, after considering the symmetry arguments, the Boltzmann equation (2.3) within the RTA (2.4) for the foliated $dS_3 \times \mathbb{R}$ reduces to

$$\frac{\partial}{\partial \rho} f^{(\kappa)}(\rho, \hat{p}_{\Sigma_\kappa}^2, \hat{p}_\zeta^2) = -\frac{\hat{T}_\kappa(\rho)}{c} \left[f^{(\kappa)}(\rho, \hat{p}_{\Sigma_\kappa}^2, \hat{p}_\zeta^2) - f_{eq}^{(\kappa)}(\hat{p}^\rho / \hat{T}_\kappa(\rho)) \right]. \quad (3.22)$$

The resulting reduced equation parallels the kinetic formulations of the Bjorken [13] and Gubser [4, 5] boost invariant flows, yet it is now written in a compact and geometrically consistent form within a given foliation leaf Σ_κ of dS_3 . Now, in Eq. (3.22) \hat{p}^ρ is the energy of the particle determined from the on-shell condition

$$\hat{p}^\rho = \sqrt{\frac{\hat{p}_{\Sigma_\kappa}^2}{S_\kappa^2(\rho)} + \hat{p}_\zeta^2} \quad (3.23)$$

where the functions $S_\kappa(\theta)$ for $\kappa = 0, \pm 1$ are listed in Table 1. The exact solution of the Boltzmann Eq. (3.22) reads as

$$f^{(\kappa)}(\rho, \hat{p}_{\Sigma_\kappa}^2, \hat{p}_\zeta^2) = D_\kappa(\rho, \rho_0) f_0^{(\kappa)}(\rho_0, \hat{p}_{\Sigma_\kappa}^2, \hat{p}_\zeta^2) + \frac{1}{c} \int_{\rho_0}^{\rho} d\rho' D_\kappa(\rho, \rho') \hat{T}_\kappa(\rho') f_{eq}^{(\kappa)}(\rho', \hat{p}_{\Sigma_\kappa}^2, \hat{p}_\zeta^2). \quad (3.24)$$

where in the previous expression the damping function $D(\rho_2, \rho_1)$ is given by

$$D_\kappa(\rho_2, \rho_1) = \exp\left(-\int_{\rho_1}^{\rho_2} d\rho'' \frac{\hat{T}_\kappa(\rho'')}{c}\right). \quad (3.25)$$

In Eqs. (3.24) and (3.25), ρ_0 is the initial “time” in $dS_3 \times \mathbb{R}$ space at which $f = f_0^{(\kappa)}(\rho_0, \hat{p}_{\Sigma_\kappa}^2, \hat{p}_\zeta)$. For simplicity, we shall assume that $f_0^{(\kappa)} \equiv f_{eq}$, where f_{eq} denotes a thermal equilibrium distribution function. This assumption can, however, be straightforwardly relaxed to describe systems far from equilibrium, as done in the conformal Bjorken [32, 33] and Gubser [36] flows. A detailed analysis of far-from-equilibrium configurations will be presented elsewhere [37].

The exact solution (3.24) constitutes the central outcome of our analysis. While it reduces to the known Bjorken [13] and Gubser [4, 5] flows for $\kappa = 0$ and $\kappa = 1$ respectively, it also unveils a new boost-invariant solution for the negatively curved foliation dS_3 ($\kappa = -1$).

4 From exact kinetics to macroscopic dynamics in $dS_3 \times \mathbb{R}$ slicings

Having obtained the exact solution of the Boltzmann equation on foliated $dS_3 \times \mathbb{R}$, we now turn to its physical implications. In this section, we evaluate the corresponding energy–momentum tensor and extract the macroscopic observables encoded in the distribution function. These results allow us to identify the hydrodynamic regime that emerges from the exact kinetics, as well as the opposite ballistic limit in which the flow becomes free streaming. Together, these analyses provide a complete characterization of the macroscopic dynamics implied by the microscopic solution.

4.1 Energy–momentum tensor from the exact solution on foliated $dS_3 \times \mathbb{R}$ geometry

The components of the energy-momentum tensor for the exact solution $f^{(\kappa)}(\rho, \hat{p}_{\Sigma_\kappa}^2, \hat{p}_\zeta)$ (3.24) can be calculated from their definitions (2.8) as follows

$$\begin{aligned} \hat{\varepsilon}_\kappa &= \langle (-u \cdot p)^2 \rangle_\kappa, \\ &= D_\kappa(\rho, \rho_0) \hat{I}_{200}(\hat{T}_{0,\kappa}; \rho, \rho_0) + \frac{1}{c} \int_{\rho_0}^\rho d\rho' \hat{T}_\kappa(\rho') D_\kappa(\rho, \rho') \hat{I}_{200}(\hat{T}_\kappa(\rho'); \rho, \rho') \end{aligned} \quad (4.1a)$$

$$\begin{aligned} \hat{\pi}^{(\kappa),\zeta} &\equiv \hat{\pi}^{(\kappa)} = \langle \hat{p}^{(\zeta)} \hat{p}_\zeta \rangle_\kappa, \\ &= D_\kappa(\rho, \rho_0) \left[\hat{I}_{020}(\hat{T}_{0,\kappa}; \rho, \rho_0) - \frac{1}{3} \hat{I}_{200}(\hat{T}_{0,\kappa}; \rho, \rho_0) \right] \\ &+ \frac{1}{c} \int_{\rho_0}^\rho d\rho' \hat{T}_\kappa(\rho') D_\kappa(\rho, \rho') \left[\hat{I}_{020}(\hat{T}_\kappa(\rho'); \rho, \rho') - \frac{1}{3} \hat{I}_{200}(\hat{T}_\kappa(\rho'); \rho, \rho') \right] \end{aligned} \quad (4.1b)$$

$$\hat{\pi}^{(\kappa),\phi} = \langle \hat{p}^{(\phi)} \hat{p}_\phi \rangle_\kappa = -\frac{\hat{\pi}^{(\kappa)}}{2}, \quad (4.1c)$$

$$\hat{\pi}^{(\kappa),\theta} = \langle \hat{p}^{(\theta)} \hat{p}_\theta \rangle_\kappa = -\frac{\hat{\pi}^{(\kappa)}}{2}. \quad (4.1d)$$

where in the previous expressions we denote the initial temperature $\hat{T}_{0,\kappa} \equiv \hat{T}_\kappa(\rho_0)$ while introducing the anisotropic integrals $\hat{I}_{nql} = \langle (\hat{p}^\rho(\rho))^n (p_\zeta)^l \left(\hat{p}_{\Sigma_\kappa}^2 / S_\kappa^2(\rho) \right)^q \rangle$ whose explicit expressions are presented in App. B. The system is conformal and thus, the equation of state is $\hat{\mathcal{P}} = \hat{\varepsilon}/3$. In addition, from Eqs. (4.1b)-(4.1d), it follows that there is only one single independent non-vanishing component⁹.

⁹Since the fluid velocity is considered in the local rest frame $\hat{u}_\mu = (-1, 0, 0, 0)$ then $\hat{u}_\mu \hat{\pi}^{\mu\nu} = 0$ such that $\hat{\pi}^{\rho\nu} = 0 \forall \nu$. The isometry group invariance over the constant curvature slice Σ_κ implies $\hat{\pi}^{ij} = 0$ for $i \neq j$.

4.1.1 Landau matching conditions

The effective temperature of the conformal gas follows from the Landau matching condition, which demands equality between the energy density of the system and that of a fictitious equilibrium state. In the Landau frame, this yields $\hat{\epsilon}_{eq.} = \hat{\epsilon}$. The equilibrium energy density given by

$$\begin{aligned}\hat{\epsilon}_{\kappa}^{eq.}(\rho, a) &= \int \frac{d^3 \hat{p}}{(2\pi)^3 S_{\kappa}^2(\rho) Q_{\kappa}(\theta)} \hat{p}^{\rho} f_{eq.}^{(\kappa)}(\hat{p}^{\rho}/\hat{T}(\rho)) \\ &= \frac{3}{\pi^2} \hat{T}_{\kappa}^4(\rho),\end{aligned}\quad (4.2)$$

where the equilibrium distribution function is $f_{eq.}(x) = e^{-x}$. Now, using Eqs. (4.1a) and (4.2), the Landau matching condition implies the following integral equation for the temperature

$$T_{\kappa}^4(\rho) = D_{\kappa}(\rho, \rho_0) \hat{R}_{200} \left(\frac{S_{\kappa}(\rho_0)}{S_{\kappa}(\rho)} \right) \hat{T}_{\kappa}^4(\rho_0) + \frac{1}{c} \int_{\rho_0}^{\rho} d\rho' \hat{R}_{200} \left(\frac{S_{\kappa}(\rho')}{S_{\kappa}(\rho)} \right) D_{\kappa}(\rho, \rho') \hat{T}_{\kappa}^5(\rho'). \quad (4.3)$$

The function \hat{R}_{200} is given explicitly in App. B, Eq. (B.5b). The integral equation (4.3) determines the temperature, which can be obtained numerically using an iterative method [4, 5, 32, 33, 38]. Once the temperature from the above equation and the full distribution function (3.24) are known, the energy–momentum tensor can be fully determined. The numerical results for foliated geometries including the Grozdanov flow solution [18] will be presented in a forthcoming publication [37].

4.2 Emergent Hydrodynamics in foliated $dS_3 \times \mathbb{R}$

Hydrodynamics arises from microscopic kinetic theory via a coarse-graining process that lifts microscopic dynamics to macroscopic fluid behavior. For the exact solution of the Boltzmann equation in an arbitrary foliation of $dS_3 \times \mathbb{R}$ (3.24), one considers the momentum moments of the distribution function and derives the corresponding equations of motion for these moments. [25]. In this section, we derive the equations of motion of the hydrodynamical variables by closely following the procedure outlined in Refs. [5, 36].

4.2.1 Ideal hydrodynamics

For the energy density $\hat{\epsilon}_{\kappa} = \langle (-\hat{u} \cdot \hat{p})^2 \rangle$ one finds the following evolution equation

$$\frac{d\hat{\epsilon}_{\kappa}}{d\rho} = \frac{d}{d\rho} \left(\langle (-u \cdot \hat{p})^2 \rangle_{\kappa} \right) \Rightarrow \frac{d \ln \hat{\epsilon}_{\kappa}}{d\rho} + R_{\kappa}(\rho) \left(\frac{8}{3} - \frac{\hat{\kappa}^{(\kappa)}}{\hat{\epsilon}_{\kappa}} \right) = 0, \quad (4.4)$$

with $R_{\kappa}(\rho) = (dS_{\kappa}(\rho)/d\rho) / S_{\kappa}(\rho)$. The ideal hydrodynamical case occurs when $\eta/S \rightarrow 0$ ($c \rightarrow 0$) so the shear stress tensor is negligible. In this limiting case, the general solution to the ideal hydrodynamical equation (4.4) reads as

$$\hat{\epsilon}_{\kappa}(\rho) = \frac{\hat{\epsilon}_{\kappa}(\rho_0)}{[S_{\kappa}(\rho)]^{8/3}} = \begin{cases} \frac{\hat{\epsilon}_1(\rho_0)}{[\cosh \rho]^{8/3}} & \kappa = 1, \\ \hat{\epsilon}_0(\rho_0) e^{8/3\rho} & \kappa = 0, \\ \frac{\hat{\epsilon}_{-1}(\rho_0)}{[\sinh \rho]^{8/3}} & \kappa = -1, \end{cases} \quad (4.5)$$

where we used explicitly the functions S_κ listed in Table 1. These results were found previously by Grozdanov [18]. Implementing the Weyl scaling to map back to Minkowski space, and applying the coordinate transformation listed in Table 2, one obtains Eqs. (2.18)–(2.20) of Ref. [18].

4.2.2 Viscous hydrodynamics

The evolution equation for the shear viscous stress tensor $\hat{\pi}_\kappa^{\mu\nu} = \langle \hat{p}^{(\mu} \hat{p}^{\nu)} \rangle_\kappa$ can also be derived from its definition (2.8c). In this case, and following Ref. [5], it is convenient to rewrite the original Boltzmann equation on foliated $dS_3 \times \mathbb{R}$ (3.22) for the deviation from equilibrium $\delta f = f^{(\kappa)} - f_{eq}^{(\kappa)}$ as follows

$$\frac{\partial \delta f_\kappa}{\partial \rho} = -\frac{\delta f_\kappa}{\hat{\tau}_r} - \frac{\partial f_{eq}^{(\kappa)}}{\partial \rho}. \quad (4.6)$$

Then, differentiating $\hat{\pi}_\kappa^{\mu\nu}$ with respect to ρ and making use of (4.6), one obtains the following evolution equation¹⁰

$$\begin{aligned} \partial_\rho \hat{\pi}_\kappa^{\mu\nu} &= \hat{\Delta}_{(\kappa),\alpha\beta}^{\mu\nu} \frac{\partial}{\partial \rho} \left(\frac{1}{(2\pi)^3} \int \frac{d^3 p}{S_\kappa^2(\rho) Q_\kappa(\theta)} \hat{p}^{(\alpha} \hat{p}^{\beta)} \right), \\ &= -\frac{\pi_\kappa^{\mu\nu}}{\tau_r} - 2 R_\kappa(\rho) \pi_\kappa^{\mu\nu} - \frac{R_\kappa(\rho)}{\hat{T}} \int_{\hat{p}} \frac{\hat{p}^{(\mu} \hat{p}^{\nu)}}{\hat{p}^\rho} \left(\frac{\hat{p}_{\Sigma_\kappa}^2}{S_\kappa^2} \right) \delta f \\ &\quad - \int_{\hat{p}} \hat{p}^{(\mu} \hat{p}^{\nu)} \left(\frac{\partial_\rho \hat{p}^\rho}{\hat{p}^\rho} \right) \delta f. \end{aligned} \quad (4.7)$$

It is sufficient to consider the $\zeta\zeta$ component of the shear stress tensor $\hat{\pi}_\kappa^{\zeta\zeta} \equiv \hat{\pi}^{(\kappa)}$ as it was demonstrated in Sect. 4.1, Eqs. (4.1b)–(4.1d). After a bit of algebra and performing some momentum integrals, one finally obtains the following integro-differential evolution equation:

$$\begin{aligned} \partial_\rho \hat{\pi}^{(\kappa)} &= -\frac{\hat{\pi}^{(\kappa)}}{\hat{\tau}_r} + \frac{4}{3} \frac{\eta}{\hat{\tau}_r} R_\kappa - \frac{46}{21} R_\kappa \hat{\pi}^{(\kappa)} \\ &\quad + \frac{R_\kappa}{3(2\pi)} \int_0^\infty d\hat{p}^\rho \int_0^{2\pi} d\theta (p^\rho)^3 \sin \theta \left(\frac{25}{21} - \cos^2 \theta \right) (3 \cos^2 \theta - 1) \delta f. \end{aligned} \quad (4.8)$$

We emphasize that the result (4.8) is exact up to second-order contributions and hence necessarily differs from more standard second-order theories such as Israel–Stewart (IS) approaches [39, 40] in which certain second-order contributions may be discarded when approximating the distribution function (see App. A of Ref. [5]). In terms of the complete result Eq. (4.8), we may then identify two distinct regimes: the Navier-Stokes limit and the limit of second-order conformal hydrodynamics.

¹⁰The Landau matching conditions imply that $\langle \hat{p}^{(\mu} \hat{p}^{\nu)} \rangle_{eq.} = 0$.

4.2.3 Navier-Stokes limit

This regime follows from Eq. (4.8) by taking the limit $\hat{\tau}_r \rightarrow 0$. Consequently, the NS shear viscous tensor reduces to

$$\hat{\pi}_{NS}^{(\kappa)} = \frac{4}{3}\eta R_\kappa = \begin{cases} \frac{4}{3}\eta \tanh \rho & \kappa = +1, \\ -\frac{4}{3}\eta & \kappa = 0, \\ \frac{4}{3}\eta \coth \rho & \kappa = -1. \end{cases} \quad (4.9)$$

Where we used the functions S_κ listed in Table 1. The NS shear viscous expressions (4.9) coincide with the results derived by Grozdanov [18]¹¹.

4.2.4 Second-order conformal hydrodynamics

If one discards the second-line contributions in Eq. (4.8), i.e., the corrections associated with the exact kinetic treatment, it leads directly to the full second-order conformal equation for the $\hat{\pi}_\kappa^{\zeta\zeta}$

$$\partial_\rho \hat{\pi}_\kappa^{\zeta\zeta} = -\frac{\hat{\pi}_\kappa^{\zeta\zeta}}{\hat{\tau}_r} + \frac{4}{3}\frac{\eta}{\hat{\tau}_r} R_\kappa - \frac{46}{21}R_\kappa \hat{\pi}_\kappa^{\zeta\zeta}. \quad (4.10)$$

It is convenient to solve the second-order differential equations for the Weyl invariant effective shear component $\bar{\pi}_\kappa = (3/4)\hat{\pi}^{(\kappa)}/\hat{\epsilon}_\kappa$. Therefore, the evolution equations of second order hydrodynamics read as

$$\frac{d \ln \hat{\epsilon}_\kappa}{d\rho} + \frac{4}{3}R_\kappa (2 - \bar{\pi}_\kappa) = 0, \quad (4.11a)$$

$$\hat{\tau}_r \left(\frac{d\bar{\pi}_\kappa}{d\rho} + \frac{4}{3}R_\kappa \bar{\pi}_\kappa^2 \right) + \bar{\pi}_\kappa = \frac{\eta}{\hat{\epsilon}_\kappa} R_\kappa + \frac{10}{21}\hat{\tau}_r R_\kappa \bar{\pi}_\kappa. \quad (4.11b)$$

Neglecting the (10/21) term in Eq. (4.11b) reduces this equation to the IS form studied in Ref. [41] for the Gubser flow and by Soloviev [42] for the Grozdanov flow. In any foliation of $dS_3 \times \mathbb{R}$ the IS evolution equation of the effective shear is

$$\text{IS theory:} \quad \hat{\tau}_r \left(\frac{d\bar{\pi}_\kappa}{d\rho} + \frac{4}{3}R_\kappa \bar{\pi}_\kappa^2 \right) + \bar{\pi}_\kappa = \frac{\eta}{\hat{\epsilon}_\kappa} R_\kappa. \quad (4.12)$$

The equation for the effective shear (4.11b) admits an analytic solution in the so-called cold limit [41]. In this regime, where the fluid is highly viscous or extremely cold - namely when $\eta/(ST) \gg 1$ - the terms proportional to $\hat{\tau}_r$ dominate in Eq. (4.11b). The effective cold limit equation for the effective shear then reads

$$c \left(\frac{d\bar{\pi}_\kappa}{d\rho} + \frac{4}{3}R_\kappa \bar{\pi}_\kappa^2 \right) = \frac{4}{3}R_\kappa + \frac{10}{21}c R_\kappa \bar{\pi}_\kappa, \quad (4.13)$$

where we used $\eta/\hat{\epsilon}_\kappa = (4/3)\hat{\tau}_r/c$ being c a constant. In the cold limit, the evolution of the shear viscous tensor reduces to a Riccati-type differential equation. The crucial difference is that Eq. (4.13) corresponds to a nonlinear *hyperbolic* Riccati flow, whereas the IS counterparts in Refs. [41, 42]

¹¹The comparison between Eqs. (4.9) and the NS solution by Grozdanov [18] is immediate once one recognizes that his result is written in terms of $\hat{\pi}^{\mu\nu} \sim \eta \hat{\sigma}^{\mu\nu}$ with $\eta = H_0 \hat{\epsilon}^{3/4}$.

fall into the *parabolic* class.¹² For any foliation of $dS_3 \times \mathbb{R}$, the resulting cold-limit approximate solution to Eq. (4.13) and the IS counterpart, $\bar{\pi}_\kappa^{\text{cold}}$ and $\bar{\pi}_\kappa^{\text{IS-cold}}$, are given by

$$\bar{\pi}_\kappa^{\text{cold}}(\rho) = \frac{\bar{\pi}_+ - \bar{\pi}_0 \bar{\pi}_- [S_\kappa(\rho)]^{-\frac{4}{3}(\bar{\pi}_+ - \bar{\pi}_-)}}{1 - \bar{\pi}_0 [S_\kappa(\rho)]^{-\frac{4}{3}(\bar{\pi}_+ - \bar{\pi}_-)}} , \quad (4.14a)$$

$$\bar{\pi}_\kappa^{\text{IS-cold}}(\rho) = \frac{1}{\sqrt{c}} \tanh \left(\frac{4}{3\sqrt{c}} [\ln S_\kappa(\rho) - \bar{\pi}_0 c] \right) , \quad (4.14b)$$

where $\bar{\pi}_0$ is an integration constant and the c -dependent fixed points of Eq. (4.13), $\bar{\pi}_\pm$, are

$$\bar{\pi}_\pm(c) = \frac{5}{28} \pm \frac{1}{28} \sqrt{25 + \frac{784}{c}} . \quad (4.15)$$

The derivation of the cold limit solutions (4.14) is presented in App. C. By inserting any of the cold-limit solutions for the effective shear (4.14) into Eq. (4.11a), one obtains the corresponding cold-limit solutions for the energy density, namely¹³

$$\hat{\varepsilon}_\kappa^{\text{cold}}(\rho) = \hat{\varepsilon}_\kappa(\rho_0) S_\kappa(\rho)^{\frac{4}{3}(\bar{\pi}_- - 2)} \left[1 - \bar{\pi}_0^{-1} (S_\kappa(\rho))^{\frac{4}{3}(\bar{\pi}_+ - \bar{\pi}_-)} \right] , \quad (4.16a)$$

$$\hat{\varepsilon}_\kappa^{\text{IS-cold}}(\rho) = \hat{\varepsilon}_\kappa(\rho_0) S_\kappa(\rho)^{-8/3} \cosh \left(\frac{4}{3\sqrt{c}} [\ln S_\kappa(\rho) - \bar{\pi}_0 c] \right) . \quad (4.16b)$$

In Fig. 1 we show the evolution of the energy density and effective shear in panels (a) and (b), respectively, for second-order hydrodynamical regimes under different approximations; a detailed description is provided in the caption. The cold limit solutions reveal a clear and unified physical picture for the energy density and effective shear across all $dS_3 \times \mathbb{R}$ foliations. In this regime, the evolution equations simplify to Riccati - type flows whose structure is dictated by the geometry of the foliation through the scale factor $S_\kappa(\rho)$. Both the full second order and the IS truncations produce shear solutions of the form $\bar{\pi}_\kappa(\rho) = \bar{\pi}_\kappa(S_\kappa(\rho))$, with the energy density inheriting the same functional dependence once the shear is substituted into the conservation law. As a consequence, the shear and the energy density exhibit parallel power law scalings governed by the expanding factor $S_\kappa(\rho)$ and, in the full second order case, by the fixed points $\bar{\pi}_\pm$ of the cold limit equation (4.13). This yields a coherent dynamical picture: the shear relaxes toward an asymptotic forward attractor (IS) or between two fixed points (full second order) as illustrated in panel (b) of Figure 1, while the energy density decays monotonically with expansion in a manner entirely determined by the same

¹²The terminology ‘parabolic’ and ‘hyperbolic’ for Riccati equations refers not to an ODE classification but to the geometric classification of one-parameter subgroups of $SL(2, \mathbb{R})$ acting projectively on $\mathbb{R}P^1$. Any Riccati equation with constant coefficients, $\pi' = a + b\pi + c\pi^2$, is the projection of a linear flow $\Psi = X\Psi$ with $X \in \mathfrak{sl}(2, \mathbb{R})$, and its solution is a Möbius transformation generated by $\exp(\rho X) \in SL(2, \mathbb{R})$ [43]. Elements of $SL(2, \mathbb{R})$ are classified by their trace: elliptic ($|\text{Tr}| < 2$), parabolic ($|\text{Tr}| = 2$), and hyperbolic ($|\text{Tr}| > 2$) [44].

¹³Since $c > 0$, the cold-limit fixed points (4.15) satisfy $\pi_+ > 0$ and $\pi_- < 0$, with $\pi_+ - \pi_- = \mathcal{O}(1)$ for typical values $c \sim 3-10$. In the cold-limit energy-density solution (4.16a), the exponent $(4/3)(\pi_- - 2)$ is strictly negative, so the leading behavior always decays with S_κ rather than blowing up. Thus any zero in the bracket $1 - \bar{\pi}_0^{-1} S_\kappa^{\frac{4}{3}(\pi_+ - \pi_-)}$ reflects only the choice of integration constant or the breakdown of the cold-limit approximation, not a physical divergence.

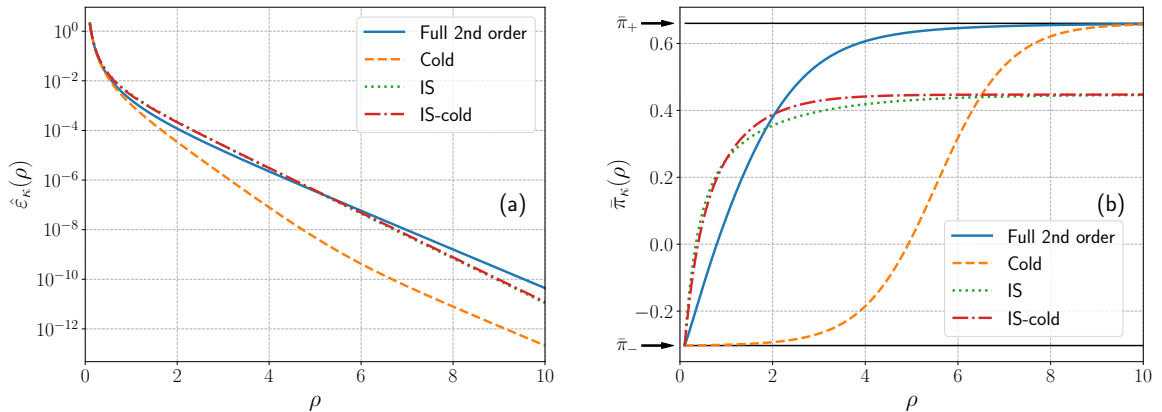


Figure 1: Comparison of viscous hydrodynamical evolution schemes for the Grozdanov flow. Panel (a): Energy density $\hat{\epsilon}_{-1}(\rho)$ and panel (b) effective shear $\bar{\pi}_{-1}(\rho)$ for four dynamical schemes: the full second-order hydrodynamic equation (solid blue line), Eqs. (4.11), its cold-limit approximation (orange long dashed), Eqs. (4.14a)-(4.16a), the Israel–Stewart (IS) equation (green dotted), Eq. (4.12), and the IS cold-limit solution (red dot-dashed), Eqs.(4.14b)- (4.16b). Panel (b) displays the relaxation of the effective shear panel (a) highlights the distinct decay rates of the energy density associated with each approximation. The initial conditions for the energy density where $\hat{\epsilon}_{-1}(\rho)$ while for the effective shear $\bar{\pi}_{-1}(\rho_0) = \bar{\pi}_{-}(c)$ (where $\bar{\pi}_{-}(c)$ is given by Eq. (4.15)) with $\rho_0 = 0.1$, $c = 5$ and $\eta/S = 0.2$.

underlying geometric and viscous parameters as shown in panel (a) of Figure 1.

We conclude this section by highlighting several features of the energy density (or temperature) evolution once viscous corrections are included in any $dS_3 \times \mathbb{R}$ foliation. For clarity, we focus on the cold-limit regime of second-order hydrodynamics, although the same conclusions extend to the full linear and nonlinear theories. A key distinction between NS and second-order hydrodynamical theories becomes evident when comparing the shear-stress and energy-density solutions in the Gubser and Grozdanov flows. In NS theory, the absence of a relaxation equation forces the shear to follow algebraically from gradients, leaving no mechanism to dynamically regulate large viscous corrections. For the maximally symmetric flows of Gubser and Grozdanov, this leads to unphysical negative temperatures in different $|\rho|$ regions. In second order hydrodynamics, by contrast, the cold limit Riccati evolution ensures that the shear remains bounded for appropriate initial conditions, which in turn guarantees physically consistent and positive energy density and temperature profiles as shown in Fig. 1. In the IS truncation, where the linear term in the Riccati equation is absent, the resulting shear flow is parabolic and exhibits a tanh-type relaxation, Eq. (4.14b), toward its forward attractor. When the linear term is retained, the full second order theory produces a hyperbolic Riccati flow interpolating between two fixed points through a Möbius transformation¹⁴. In both cases, the bounded nature of the shear prevents the NS pathology, a feature also reflected in the

¹⁴A Möbius, or fractional linear, transformation is a map of the form

$$f(x) = \frac{Ax + B}{Cx + D}$$

with $AD - BC \neq 0$. In the cold limit solution of Eq. (4.14a) this structure appears with $x = (S_{\kappa}(\rho))^{-\frac{4}{3}(\bar{\pi}_{+} - \bar{\pi}_{-})}$.

improved behavior of Gubser flow within the causal first order NS theory of Bemfica, Disconzi, and Noronha [45]. In this formulation, the evolution equations remain regular and avoid the emergence of negative temperatures - an indication of the breakdown of the Landau frame - while still reproducing the qualitative IS-like regulation of dissipative corrections.

4.3 Free streaming in $dS_3 \times \mathbb{R}$ slices

A particularly relevant regime in kinetic theory occurs when the expansion rate exceeds the collision rate, driving the system into the non-hydrodynamic free-streaming propagation. In the RTA model, this limit is realized by assuming an infinitely long relaxation time, effectively taking $\eta/S \rightarrow \infty$ ($c \rightarrow \infty$) so only the first term in the RHS of Eq. (3.24) contributes. In this regime, the energy density (4.1a) and $\zeta\zeta$ component of the shear stress (4.1b) simplify to the following expressions

$$\hat{\epsilon}_\kappa^{f.s.} = \hat{I}_{200}(\hat{T}_{0,\kappa}; \rho, \rho_0), \quad (4.17a)$$

$$\hat{\pi}_{f.s.}^{(\kappa)} = \left[\hat{I}_{020}(\hat{T}_{0,\kappa}; \rho, \rho_0) - \frac{1}{3} \hat{I}_{200}(\hat{T}_{0,\kappa}; \rho, \rho_0) \right]. \quad (4.17b)$$

The numerical studies of the free streaming regime and its validity range for a given foliation of $dS_3 \times \mathbb{R}$ will be discussed in a forthcoming publication [37].

5 From foliated $dS_3 \times \mathbb{R}$ to Minkowski $\mathbb{R}^{3,1}$

Table 2: Coordinate transformations $\rho(\tau, r)$ and $\theta(\tau, r)$, together with the corresponding Milne coordinate ranges $x^\mu = (\tau, r, \phi, \zeta)$ in $\mathbb{R}^{3,1}$ for different spatial curvatures according to Ref. [18]. In all the cases $0 < r < \infty$, $0 \leq \phi < 2\pi$ and $-\infty < \zeta < \infty$.

κ	$\rho(\tau, r)$	$\theta(\tau, r)$	τ range
0	$\ln \tau$	r	$0 < \tau < \infty$
+1	$\operatorname{arcsinh} \left(-\frac{1-q^2(\tau^2-r^2)}{2q\tau} \right)$	$\arctan \left(\frac{2qr}{1+q^2(\tau^2-r^2)} \right)$	$0 < \tau < \infty$
-1	$\operatorname{arccosh} \left(\frac{1+q^2(\tau^2-r^2)}{2q\tau} \right)$	$\operatorname{arctanh} \left(\frac{2qr}{1-q^2(\tau^2-r^2)} \right)$	$\frac{1}{q} < \tau - r$

Under a Weyl rescaling, a tensor $Q_{v_1 \dots v_n}^{\mu_1 \dots \mu_m}$ of rank (m, n) transforms as [46]

$$Q_{v_1 \dots v_n}^{\mu_1 \dots \mu_m} \longrightarrow \Omega^{\Delta+m-n}(x) Q_{v_1 \dots v_n}^{\mu_1 \dots \mu_m}, \quad (5.1)$$

where Δ is the canonical dimension and $\Omega(x)$ is the Weyl factor. For all three constant-curvature slicings considered in Sect. 3.1, the conformal map between Minkowski space $\mathbb{R}^{3,1}$ and a given $dS_3 \times \mathbb{R}$ foliation is implemented by the Weyl rescaling

$$d\hat{s}_{dS_3 \times \mathbb{R}}^2 = \frac{1}{\tau^2} dS_{\mathbb{R}^{3,1}}^2, \quad (5.2)$$

from which we identify the Weyl factor as $\Omega(\tau, r) = \tau^{-1}$. In addition to this scaling, the full conformal map to a particular $dS_3 \times \mathbb{R}$ slice requires a coordinate transformation of the form $\hat{x}^\mu =$

$\hat{x}^\mu(\tau, r; \kappa)$. The combined Weyl and coordinate transformations, together with the corresponding coordinate ranges for each slicing, are summarized in Table 2 [18].

For clarity, we further depict the foliations and their corresponding coordinate relations in Fig. 2. In the lefthand panels of Fig. 2, we show foliations of the de Sitter hyperboloid (blue surface) at constant X^0 (Gubser - top), constant $X^3 - X^0$ (Bjorken - middle), and constant X^3 (Grozdanov - bottom), each with a representative leaf from that foliation (green planes) and its intersection with the hyperboloid (solid red curves). The dashed red curves similarly display intersections of the hyperboloid with other leaves (not shown) from the same foliation. One observes that leaves in the Gubser ($\kappa = +1$) foliation yield compact geometries which are parametrized by $0 \leq \theta \leq 2\pi$, whereas the Bjorken ($\kappa = 0$) and Grozdanov ($\kappa = -1$) foliations correspond to open geometries which are either parabolic or hyperbolic, respectively, such that $0 \leq \theta \leq \infty$, consistent with the ranges given in Table 1. Each geometry thus reflects the constant curvature κ of the corresponding foliation. In the righthand panels of Fig. 2, we visualize the relations between the foliated dS_3 coordinates (ρ, θ) and the usual Milne coordinates (τ, r) , with the explicit coordinate transformations provided in Table 2. Whereas the Bjorken coordinates (middle) relate trivially to the corresponding de Sitter coordinates, the Gubser (top) and Grozdanov (bottom) coordinates map non-trivially onto Milne coordinates. In all foliations, increasing ρ at $r = 0$ coincides with increasing τ , while taking $\theta \rightarrow 0$ is equivalent to taking $r \rightarrow 0$. Likewise, in the Gubser and Bjorken foliations, one finds that increasing θ at $\tau = 0$ is equivalent to increasing r , whereas the Grozdanov foliation tends toward the limiting line $q\tau = qr + 1$ as $\theta \rightarrow +\infty$ or $\rho \rightarrow 0$.

5.1 Interpreting Slice-depending Casimirs in Minkowski Space

In Sec. 3.4.1, we determined the Casimirs of a given $dS_3 \times \mathbb{R}$, Eqs. (3.18) and (3.19), and provided their geometric interpretation. To clarify their physical content, in this section we rewrite these invariants in terms of momenta measured in ordinary Minkowski space. This makes explicit how the conserved quantities on curved slices correspond to boosted and Weyl-rescaled combinations of Minkowski momentum. In this way, the Casimirs provide a unified interpretation of all boost-invariant flows through the geometry of their underlying slicings. We follow closely the approach of Ref. [47].

5.1.1 Momentum transformation and radial-boost structure

The combination of the Weyl factor and the coordinate transformation between $\mathbb{R}^{3,1}$ and $dS_3 \times \mathbb{R}$ slicings leads to the general momentum transformation

$$\hat{p}^\mu = \Omega(x)^{-2} \left(\frac{\partial \hat{x}^\mu}{\partial x^\alpha} \right) p^\alpha \quad (5.3)$$

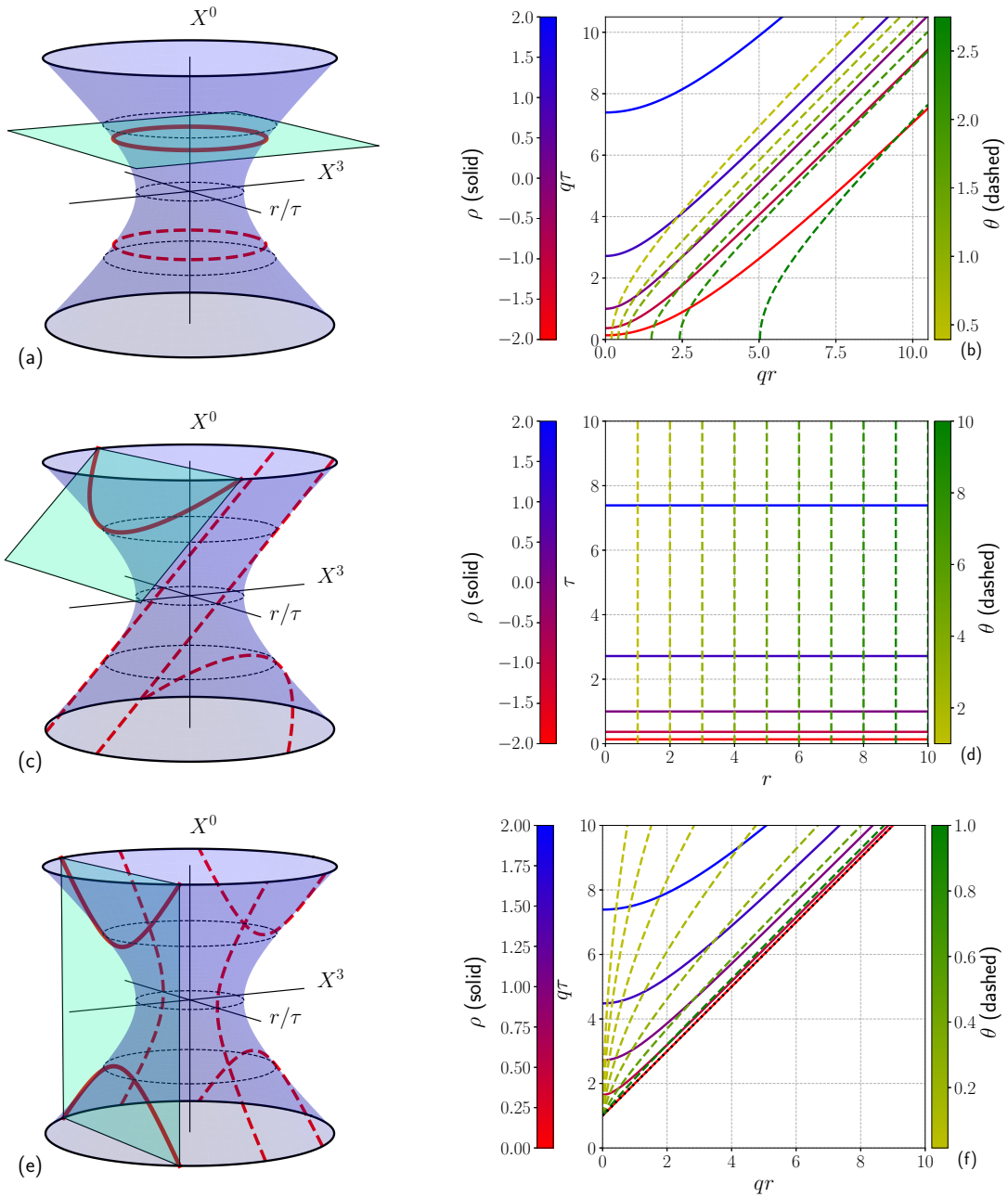


Figure 2: Different choices of foliation of $dS_3 \times \mathbb{R}$, parameterized by (ρ, θ) , and the corresponding relations to Milne coordinates (τ, r) . **Left panels:** The Gubser solution (top row; $\kappa = +1$) corresponds to foliations at $X^0 = \text{constant}$; the Bjorken solution (middle row; $\kappa = 0$) is defined by foliating with $X^3 - X^0 = \text{constant}$; and the Grozdanov solution (bottom row; $\kappa = -1$) reflects foliations with respect to $X^3 = \text{constant}$. Intersections between the chosen level and the hyperboloid are displayed as solid red contours, while other levels are displayed as dashed red contours. Black dashed contours at constant X^0 are included to help visualize the hyperboloid. **Right panels:** relations between (ρ, θ) and (τ, r) for each foliation. The ranges shown for ρ and θ in each panel are chosen solely for aesthetic purposes; the full ranges are given in 1.

The explicit coordinate mapping is

$$\hat{p}^\rho = \tau^2 \left(\frac{\partial \rho}{\partial \tau} p^\tau + \frac{\partial \rho}{\partial r} p^r \right), \quad (5.4)$$

$$\hat{p}^\theta = \tau^2 \left(\frac{\partial \theta}{\partial \tau} p^\tau + \frac{\partial \theta}{\partial r} p^r \right), \quad (5.5)$$

$$\hat{p}^\phi = \tau^2 p^\phi, \quad (5.6)$$

$$\hat{p}^\zeta = \tau^2 p^\zeta. \quad (5.7)$$

For the Gubser and Grozdanov flows, the fluid velocity in $dS_3 \times \mathbb{R}$ is static, whereas in Minkowski space u^μ is purely radial and azimuthally symmetric, so $u^\mu(\tau, r) = (u^\tau(\tau, r), u^r(\tau, r), 0, 0)$ which we parametrize as

$$u^\tau = \gamma_\kappa(\tau, r), \quad u^r = \gamma_\kappa(\tau, r) v_\kappa(\tau, r), \quad (5.8)$$

with $\gamma_\kappa = 1/\sqrt{1 - v_\kappa^2}$. Using the Weyl transformation of vectors¹⁵, $\hat{u}^\mu = \Omega^{-1} (\partial \hat{x}^\mu / \partial x^\alpha) u^\alpha$ leads to the following equations

$$\tau \partial_\tau \rho \gamma_\kappa + \tau \partial_r \rho \gamma_\kappa v_\kappa = 1, \quad (5.9)$$

$$\tau \partial_\tau \theta \gamma_\kappa + \tau \partial_r \theta \gamma_\kappa v_\kappa = 0. \quad (5.10)$$

Solving these equations yields the Jacobian derivatives in terms of the radial boost,

$$\begin{aligned} \tau \partial_\tau \rho &= \gamma_\kappa, & \tau \partial_r \rho &= -\gamma_\kappa v_\kappa, \\ \tau \partial_\tau \theta &= -\frac{\gamma_\kappa v_\kappa}{S_\kappa(\rho)}, & \tau \partial_r \theta &= \frac{\gamma_\kappa}{S_\kappa(\rho)}. \end{aligned} \quad (5.11)$$

Substituting (5.11) back into the momentum transformation (5.4) yields to the following general transformation for any constant-curvature slicing ($\kappa = \pm 1$),

$$\begin{aligned} \hat{p}^\rho &= \tau \gamma_\kappa(\tau, r) (p^\tau - v_\kappa(\tau, r) p^r), \\ \hat{p}^\theta &= \frac{\gamma_\kappa(\tau, r)}{S_\kappa(\rho(\tau, r))} (p^r - v_\kappa(\tau, r) p^\tau), \\ \hat{p}^\phi &= \tau^2 p^\phi, \quad \hat{p}^\zeta = \tau^2 p^\zeta. \end{aligned} \quad (5.12)$$

Therefore, we can understand the particle's momenta in $dS_3 \times \mathbb{R}$ in terms of momenta in the lab frame boosted by a radial flow.

¹⁵Note that the Weyl weights of the fluid velocity \hat{u}^μ and \hat{p}^μ differ: the four-velocity is rescaled with Ω^{-1} so as to preserve the normalization $\hat{u}_\mu \hat{u}^\mu = -1$, whereas the momentum acquires an extra factor Ω^{-2} because the canonical covector p_μ is taken as Weyl-invariant and indices are raised with the rescaled metric $\hat{g}^{\mu\nu} = \Omega^{-2} g^{\mu\nu}$.

5.1.2 Casimirs in terms of boosted momenta

Using Eqs. (5.12) allows to rewrite the Casimir associated with the constant-curvature slice Σ_κ , Eq. (3.18), in terms of Minkowski momenta as follows

$$\hat{C}_\kappa = \hat{p}_\theta^2 + \frac{\hat{p}_\phi^2}{Q_\kappa^2(\theta)} \Rightarrow C_\kappa = \frac{\gamma_\kappa^2}{S_\kappa^2(\rho)} (p^r - v_\kappa p^\tau)^2 + \frac{\tau^4 (p^\phi)^2}{Q_\kappa^2(\theta)}. \quad (5.13)$$

Now, without losing any generality, we shall assume that for an azimuthally symmetric flow $p^\phi = 0$. For $\kappa = +1$ (spherical slicing, Gubser flow) one has $S_{+1}(\rho) = \cosh \rho$ and $Q_{+1}(\theta) = \sin \theta$ (see Table 1). the Casimir reduces to

$$C_{+1} = \frac{\gamma_{+1}^2}{\cosh^2 \rho} (p^r - v_{+1} p^\tau)^2, \quad (5.14)$$

which is equivalent to Eq. (15) of Ref. [47] after expressing p^r through the transverse momentum p_T .

For $\kappa = -1$ (hyperbolic slicing, ‘‘Grozdanov flow’’), one has that the hyperbolic scale factor $S_{-1}(\rho) = \sinh \rho$, leading to

$$C_{-1} = \frac{\gamma_{-1}^2}{\sinh(\rho(\tau, r))} (p^r - v_{-1} p^\tau)^2 \quad (5.15)$$

which represents the invariant momentum norm on the hyperbolic plane H^2 - the geodesic distance in the metric $ds^2 = d\theta^2 + \sinh^2 \theta d\phi^2$, and constitutes the characteristic invariant of the Grozdanov flow - written entirely in terms of Minkowski momenta and the radial velocity field $v_{-1}(\tau, r)$. In our upcoming work [37], we will numerically assess the physical conditions that delimit the validity and applicability of the novel kinetic solution for the Grozdanov flow.

Notice that for the $\kappa = 0$, one can still use the general transformation between momenta in $dS_3 \times \mathbb{R}$ and $\mathbb{R}^{3,1}$, Eqs. (5.4), by setting $v_0(\tau, r) = 0$. In that case it is straightforward to show that the Casimir C_0 is simply the transverse momentum of the particle, namely

$$C_0 = p_T^2 = p_r^2 + \frac{p_\phi^2}{r^2}, \quad (5.16)$$

where we used explicitly the function $Q_0(\theta) = \theta \equiv r$ [18]. This result follows purely from the flat $ISO(2)$ symmetry of the transverse plane for the Bjorken flow. Finally, the Casimir C_ζ associated to \mathbb{E}_1 is identified as the longitudinal momentum which follows directly from Eqs. (5.12).

6 Conclusions

In this work we have developed a unified formulation of relativistic kinetic theory for an uncharged conformal gas evolving on arbitrary foliations of $dS_3 \times \mathbb{R}$. By exploiting the maximal symmetry of dS_3 and its different constant-curvature slicings, we obtained a single exact solution of the Boltzmann equation whose restriction to specific foliations reproduces the Bjorken [13] and Gubser [4, 5] kinetic solutions, and, in addition, yields a new exact kinetic solution describing a gas undergoing Grozdanov flow. Thus all three expanding systems arise as different coordinate projections of one

underlying invariant hyperboloid, exposing a unifying geometric origin for a broad class of kinetic solutions that would otherwise appear unrelated.

Our formulation makes systematic use of the cotangent bundle description of kinetic theory and its geometric representation in the phase space [19–24]. This perspective brings to the forefront the roles of symmetry generators, Casimir invariants, and momentum maps in constructing exact solutions of the Boltzmann equation. It also highlights the intrinsic foliation–independence of the distribution function: once lifted to the cotangent bundle, the kinetic solution acquires a representation that does not privilege any particular slicing of dS_3 . Consequently, emergent hydrodynamic behavior—ideal, viscous, or free streaming—can be analyzed uniformly across all foliations simply by projecting the same exact kinetic solution onto different hypersurfaces. In addition to the exact Boltzmann solution for a system undergoing Grozdanov flow, we have also obtained new approximate solutions for second–order hydrodynamic theories in the so-called cold limit [41], now implemented on arbitrary $dS_3 \times \mathbb{R}$ foliations rather than only the Gubser geometry. The cold–limit analysis demonstrates how geometric properties of the foliation govern the relaxation of viscous stresses and the corresponding evolution of the energy density.

In addition to unifying existing flows, the geometric structure inherent in the cotangent-bundle formulation provides a flexible framework for identifying new exact solutions in systems with suitable symmetries and for probing far–from–equilibrium dynamics. More broadly, this geometric viewpoint opens new avenues for studying non-equilibrium attractors, symmetry-protected transport, and universal features of out-of-equilibrium evolution directly within kinetic theory.

In a forthcoming follow–up work [37], we will examine the numerical properties of the exact solutions of the Boltzmann equation in different foliated geometries for far-from equilibrium situations, with particular emphasis on the structure induced by Grozdanov flow and its implications for hydrodynamization, causality and stability.

Acknowledgments

We thank to Sašo Grozdanov for useful conversations about his novel hydrodynamical solution [18]. We are also grateful to Olivier Sarbach for useful correspondence about the cotangent bundle formulation approach to relativistic kinetic theory. M. M. thanks to C. Taepke-Guerrero for contributing to a creative, harmonious and productive working environment during the completion of this work.

A Killing vectors of a 2d constant curvature manifold

In this section, we outline some relevant results used in Sec. 2 which can be derived from standard methods of differential geometry [48, 49]. The maximally symmetric submanifold $\Sigma_\kappa \subset dS_3 \times \mathbb{R}$ with constant spatial curvature κ is parameterized by coordinates (θ, ϕ) . Its induced metric is

$$d\Sigma_\kappa^2 = h_{ij} dx^i dx^j = d\theta^2 + Q_\kappa^2(\theta) d\phi^2. \quad (\text{A.1})$$

Equation (A.1) describes the canonical geometry of a two-dimensional space form of curvature κ , corresponding, respectively, to a sphere \mathbb{S}^2 ($\kappa = 1$), an euclidian plane \mathbb{R}^2 ($\kappa = 0$), or a hyperbolic plane \mathbb{H}^2 ($\kappa = -1$), embedded in dS_3 . For the induced metric (A.1) the non-zero Christoffel

symbols are

$$\Gamma_{\phi\phi}^\theta = -Q_\kappa(\theta)Q'_\kappa(\theta), \quad \Gamma_{\theta\phi}^\phi = \Gamma_{\theta\phi}^\theta = \frac{Q'_\kappa(\theta)}{Q_\kappa(\theta)} \equiv G_\kappa(\theta). \quad (\text{A.2})$$

In a two dimensional manifold, the Ricci scalar and the Gaussian curvatures are related by simply $\mathcal{R} = 2\kappa$ [48, 49]. For the metric (A.1) this relation implies the following differential equation

$$Q''_\kappa + \kappa Q_\kappa(\theta) = 0, \quad \Rightarrow \quad (Q'_\kappa)^2 + \kappa Q_\kappa^2 = 1, \quad (\text{A.3})$$

Notice that, by solving the previous differential equation for $\kappa = \{1, 0, -1\}$, corresponding to spherical, flat, and hyperbolic geometries respectively, and using as initial conditions $\{Q(0) = 0, Q'_\kappa = 1\}$, one obtains the three functions Q_κ listed in Table 1. For the case $\kappa = 1$, the resulting induced metric (A.1) is maximally symmetric under $\mathfrak{so}(3)$. Consequently, one can anticipate that the induced metric h_{ij} in Eq. (A.1) admits a maximally symmetric three-dimensional isometry algebra, corresponding to three independent Killing vectors.

On the two-dimensional submanifold $\Sigma_\kappa \subset dS_3 \times \mathbb{R}$ with local coordinates (θ, ϕ) , any tangent vector field can be expressed in components as

$$\hat{\mathcal{K}}_A^{(\kappa)} = \sum_{i=1}^2 \hat{\mathcal{K}}_A^{i,(\kappa)} e_i = \hat{\mathcal{K}}_A^{\theta,(\kappa)}(\theta, \phi) e_\theta + \hat{\mathcal{K}}_A^{\phi,(\kappa)}(\theta, \phi) e_\phi \quad \text{with } (e_\theta, e_\phi) = (\partial_\theta, \partial_\phi), \quad (\text{A.4})$$

where the coordinate vectors $(\partial_\theta, \partial_\phi)$ form a local basis in the tangent space $\mathcal{T}_p\Sigma_\kappa$ at each point p . The Killing equations [48, 49], $\nabla_i \mathcal{K}_j + \nabla_j \mathcal{K}_i = 0$, give the following set of coupled PDEs

$$(\theta\theta) : \quad \partial_\theta \hat{\mathcal{K}}_{A,\theta}^{(\kappa)} = 0, \quad \Rightarrow \quad \hat{\mathcal{K}}_{A,\theta}^{(\kappa)} = \hat{\mathcal{K}}_{A,\theta}^{(\kappa)}(\phi), \quad (\text{A.5a})$$

$$(\theta\phi) : \quad \partial_\phi \hat{\mathcal{K}}_{A,\theta}^{(\kappa)} + \partial_\theta (Q_\kappa^2(\theta) \hat{\mathcal{K}}_{A,\phi}^{(\kappa)}) - 2G_\kappa(\theta) Q_\kappa^2(\theta) \hat{\mathcal{K}}_{A,\phi}^{(\kappa)} = 0, \quad (\text{A.5b})$$

$$(\phi\phi) : \quad \partial_\phi (Q_\kappa^2(\theta) \hat{\mathcal{K}}_{A,\phi}^{(\kappa)}) + G_\kappa(\theta) Q_\kappa^2(\theta) \hat{\mathcal{K}}_{A,\phi}^{(\kappa)} = 0. \quad (\text{A.5c})$$

Since $0 \leq \phi \leq 2\pi$ (see Table 1), the most general solution¹⁶ of Eq. (A.5a) is

$$\hat{\mathcal{K}}_{A,\theta}^{(\kappa)}(\phi) = \alpha \cos(\phi) + \beta \sin(\phi) + \gamma. \quad (\text{A.6})$$

where α , β and γ are constants to be determined. It follows from this expression that, to satisfy Eq. (A.5c), $\hat{\mathcal{K}}_{A,\phi}^{(\kappa)}$ must take the following generic functional form

$$\hat{\mathcal{K}}_{A,\phi}^{(\kappa)}(\theta, \phi) = u(\theta) \sin \phi + v(\theta) \cos \phi + b_0(\theta). \quad (\text{A.7})$$

Inserting this into Eq. (A.5c) yields

$$u(\theta) = -G_\kappa(\theta)\alpha, \quad v(\theta) = G_\kappa(\theta)\beta, \quad (\text{A.8})$$

¹⁶In principle, the most general solution would also include higher order harmonics as well, such as $\alpha_n \cos(n\phi) + \beta_n \sin(n\phi)$ with $n > 1$. However, one finds in this case that the two remaining equations (A.5b)-(A.5c) cannot be solved simultaneously when these higher order terms are included.

so that

$$\hat{\mathcal{K}}_{A,\phi}^{(\kappa)}(\theta, \phi) = -G_\kappa(\theta)\alpha \sin \phi + G_\kappa(\theta)\beta \cos \phi + b_0(\theta). \quad (\text{A.9})$$

Substituting (A.9) into (A.5b) and equating the coefficients of $\sin \phi$, $\cos \phi$, and the constant term yields two independent conditions:

$$-1 - (Q_\kappa Q'_\kappa)' + 2G_\kappa Q_\kappa Q'_\kappa = 0, \quad (\text{A.10a})$$

$$(Q_\kappa^2 b_0)' - 2G_\kappa Q_\kappa^2 b_0 = 0. \quad (\text{A.10b})$$

Using $(Q_\kappa Q'_\kappa)' = (Q'_\kappa)^2 + Q_\kappa Q''_\kappa$ and $G_\kappa Q_\kappa Q'_\kappa = (Q'_\kappa)^2$, the first condition (A.10a) simplifies to

$$-1 + (Q'_\kappa)^2 - Q_\kappa Q''_\kappa = 0. \quad (\text{A.11})$$

For a surface of constant curvature, the metric function $Q_\kappa(\theta)$ satisfies (A.3); substituting these into (A.11) gives $-1 + (Q'_\kappa)^2 - Q_\kappa Q''_\kappa = -1 + (Q'_\kappa)^2 + \kappa Q_\kappa^2 = 0$, so condition (A.11) holds identically. Hence, no additional restriction arises on the constants α, β . The second condition (A.10b) integrates directly to $Q_\kappa^2 b_0' = 0 \Rightarrow b_0(\theta) = \text{const}$. Finally, the constant term γ in $\hat{\mathcal{K}}_{A,\phi}^{(\kappa)}$ (A.6) must vanish from (A.5c). Indeed, with $\gamma \neq 0$, the first term in the RHS of Eq. (A.5c) is 2π -periodic and its average over ϕ vanishes, while $Q_\kappa Q'_\kappa \gamma$ is ϕ -independent. Therefore, consistency requires $Q_\kappa Q'_\kappa \gamma = 0$, implying $\gamma = 0$.

Summarizing, the components of the most general Killing vector field (A.4) for the induced metric (A.1) are

$$\hat{\mathcal{K}}_{A,\theta}^{(\kappa)}(\phi) = \alpha \cos \phi + \beta \sin \phi, \quad (\text{A.12})$$

$$\hat{\mathcal{K}}_{A,\phi}^{(\kappa)}(\theta, \phi) = -G_\kappa(\theta)\alpha \sin \phi + G_\kappa(\theta)\beta \cos \phi + b_0, \quad (\text{A.13})$$

with constants α, β, b_0 . Choosing the triplets $(\alpha, \beta, b_0) = (1, 0, 0), (0, 1, 0), (0, 0, 1)$ gives the canonical basis

$$\begin{aligned} \hat{\mathcal{K}}_1^{(\kappa)}(\theta, \phi, \kappa) &= \cos \phi \partial_\theta - G_\kappa(\theta) \sin \phi \partial_\phi, \\ \hat{\mathcal{K}}_2^{(\kappa)}(\theta, \phi, \kappa) &= \sin \phi \partial_\theta + G_\kappa(\theta) \cos \phi \partial_\phi, \\ \hat{\mathcal{K}}_3^{(\kappa)}(\theta, \phi, \kappa) &= \partial_\phi. \end{aligned} \quad (\text{A.14})$$

A.1 Lie algebra

Given the three Killing vectors (A.14), we determine their algebraic structure by explicitly evaluating the Lie bracket between different pairs of Killing vectors as follows

- $[\hat{\mathcal{K}}_3^{(\kappa)}, \hat{\mathcal{K}}_1^{(\kappa)}]:$

$$\begin{aligned} [\hat{\mathcal{K}}_3^{(\kappa)}, \hat{\mathcal{K}}_1^{(\kappa)}] &= \partial_\phi(\cos \phi) \partial_\theta - G_\kappa(\theta) \partial_\phi(\sin \phi) \partial_\phi, \\ &= -(\sin \phi \partial_\theta + G_\kappa(\theta) \cos \phi \partial_\phi) \equiv -\hat{\mathcal{K}}_2^{(\kappa)}. \end{aligned} \quad (\text{A.15})$$

- $[\hat{\mathcal{K}}_3^{(\kappa)}, \hat{\mathcal{K}}_2^{(\kappa)}]:$

$$\begin{aligned} [\hat{\mathcal{K}}_3^{(\kappa)}, \hat{\mathcal{K}}_1^{(\kappa)}] &= \partial_\phi (\sin \phi) \partial_\theta + G_\kappa(\theta) \partial_\phi (\cos \phi) \partial_\phi, \\ &= (\cos \phi \partial_\theta - G_\kappa(\theta) \sin \phi \partial_\phi) \equiv \hat{\mathcal{K}}_1^{(\kappa)}. \end{aligned} \quad (\text{A.16})$$

- $[\hat{\mathcal{K}}_1^{(\kappa)}, \hat{\mathcal{K}}_2^{(\kappa)}]:$

$$\begin{aligned} [\hat{\mathcal{K}}_1^{(\kappa)}, \hat{\mathcal{K}}_2^{(\kappa)}] &= \underbrace{(\hat{\mathcal{K}}_1^{(\kappa)}(\sin \phi) - \hat{\mathcal{K}}_2^{(\kappa)}(\cos \phi))}_{\equiv 0} \partial_\theta \\ &+ (\hat{\mathcal{K}}_1^{(\kappa)}(G_\kappa(\theta) \cos \phi) + \hat{\mathcal{K}}_2^{(\kappa)}(G_\kappa(\theta) \sin \phi)) \partial_\phi, \\ &= (G'_\kappa(\theta) + G_\kappa^2(\theta)) \partial_\phi, \\ &= -\kappa \partial_\phi \equiv -\kappa \hat{\mathcal{K}}_3^{(\kappa)}, \end{aligned} \quad (\text{A.17})$$

where in the third line we used (A.3).

In summary, the Killing vectors of a 2d constant curvature surface satisfy the following non-abelian Lie algebra

$$[\hat{\mathcal{K}}_1^{(\kappa)}, \hat{\mathcal{K}}_2^{(\kappa)}] = -\kappa \hat{\mathcal{K}}_3^{(\kappa)}, \quad [\hat{\mathcal{K}}_2^{(\kappa)}, \hat{\mathcal{K}}_3^{(\kappa)}] = -\hat{\mathcal{K}}_1^{(\kappa)}, \quad [\hat{\mathcal{K}}_3^{(\kappa)}, \hat{\mathcal{K}}_1^{(\kappa)}] = -\hat{\mathcal{K}}_2^{(\kappa)}, \quad (\text{A.18})$$

The structure constants can be read directly from the commutation relations, yielding

$$\{f_{12}^3, f_{23}^1, f_{31}^2\} = \{-\kappa, -1, -1\}. \quad (\text{A.19})$$

Depending on the curvature parameter κ , the non-abelian Lie algebra (A.18) corresponds respectively to $\mathfrak{so}(3)$, $\mathfrak{iso}(2)$ and $\mathfrak{so}(2, 1)$ algebras for $\kappa = \{1, 0, -1\}$. Notably, one of the structure constants depends explicitly on the spatial curvature κ of the 2d submanifold Σ_κ emphasizing the deep correspondence between geometry and its associated algebraic structure. This dependence exemplifies how curvature encodes itself in the commutation relations of the symmetry generators.

B Anisotropic integrals

The computation of the energy–momentum tensor for the exact solution of the Boltzmann equation, Eq. (3.24), requires evaluating several angular momentum integrals that appear naturally within the framework of anisotropic hydrodynamics (cf. Ref. [36]). For completeness, we collect here the key integrals used throughout this work. The anisotropic integrals \hat{I}_{nlq} are defined as

$$\hat{I}_{nlq} = \int_{\hat{p}(\rho)} (\hat{p}^\rho(\rho))^n (\hat{p}_\zeta)^l \left(\frac{\hat{p}_{\Sigma_\kappa}^2}{S_\kappa^2(\rho)} \right)^q f_{eq.}^{(\kappa)} \left(\frac{\hat{p}^\rho(\rho_0)}{\hat{T}_\kappa(\rho_0)} \right), \quad (\text{B.1})$$

with $\hat{T}_{0,\kappa} \equiv \hat{T}_\kappa(\rho_0)$ and we are considering a generic equilibrium distribution function $f_{eq.}(x) = e^{-x}$. In addition, the ρ -dependent measure is $\int_{\hat{p}(\rho)} \equiv \int d^3 \hat{p} / [(2\pi)^3 S_\kappa(\rho) Q_\kappa(\theta) \hat{p}^\rho]$. Upon the following

change of variables

$$\frac{\hat{p}_\theta}{S_\kappa(\rho_0)} = \hat{T}_{0,\kappa} \lambda \sin \alpha \cos \beta, \quad (\text{B.2a})$$

$$\frac{\hat{p}_\phi}{S_\kappa(\rho_0) Q_\kappa(\theta)} = \hat{T}_{0,\kappa} \lambda \sin \alpha \sin \beta, \quad (\text{B.2b})$$

$$\hat{p}_\zeta = \hat{T}_{0,\kappa} \lambda \cos \alpha, \quad (\text{B.2c})$$

the integral (B.1) factorizes as follows

$$\hat{I}_{nlq}(\hat{T}_{0,\kappa}; \rho, \rho_0) = \hat{J}_{nlq}(\hat{T}_{0,\kappa}) \hat{R}_{nlq} \left(\left[\frac{S_\kappa(\rho_0)}{S_\kappa(\rho)} \right]^2 \right), \quad (\text{B.3})$$

where the functions \hat{J}_{nlq} and \hat{R}_{nlq} are given by

$$\hat{J}_{nlq}(\hat{T}_{0,\kappa}) = \frac{\Gamma(n+l+2q+2)}{2\pi^2} \hat{T}_{0,\kappa}^{n+l+2q+2}, \quad (\text{B.4a})$$

$$\hat{R}_{nlq}(y) = \frac{y^2}{2} \int_{-1}^1 dx [y^2(1-x^2) + x^2]^{(n-1)/2} x^l [y^2(1-x^2)]^{2q}. \quad (\text{B.4b})$$

The integrals needed in this work are $\hat{I}_{200} = \hat{J}_{200}(\hat{T}_{0,\kappa}) \hat{R}_{200}(y)$ and $\hat{I}_{020} = \hat{J}_{020}(\hat{T}_{0,\kappa}) \hat{R}_{020}(y)$ - being $y = S_\kappa(\rho_0)/S_\kappa(\rho)$ - where the \hat{J} and \hat{R} functions are

$$\hat{J}_{200}(\hat{T}_{0,\kappa}) = \hat{J}_{020}(\hat{T}_{0,\kappa}) = \frac{3}{\pi^2} \hat{T}_{0,\kappa}^4, \quad (\text{B.5a})$$

$$\hat{R}_{200}(y) = \frac{y^2}{2} \left(1 + y^2 \frac{\tanh^{-1}(\sqrt{1-y^2})}{\sqrt{1-y^2}} \right), \quad (\text{B.5b})$$

$$\hat{R}_{020}(y) = \frac{1}{2} y^2 \left(\frac{1}{1-y^2} - y^2 \frac{\tanh^{-1}(\sqrt{1-y^2})}{(1-y^2)^{3/2}} \right). \quad (\text{B.5c})$$

C The approximate cold-limit solution

In this appendix, we solve the differential equation Eq. (4.13):

$$c \left[\frac{d\bar{\pi}^{(\kappa)}}{d\rho} + \frac{4}{3} (\bar{\pi}^{(\kappa)}(\rho))^2 R_\kappa(\rho) \right] = \frac{4}{3} R_\kappa(\rho) + \frac{10}{21} c R_\kappa(\rho) \bar{\pi}^{(\kappa)}(\rho), \quad (\text{C.1})$$

for an arbitrary known Hubble-like scale factor $R_\kappa(\rho) = (1/S_\kappa(\rho))(dS_\kappa/d\rho)$. Introducing the logarithmic scale variable

$$u(\rho) \equiv \int^\rho R_\kappa(\rho') d\rho' = \ln S_\kappa(\rho) + \text{const}, \quad (\text{C.2})$$

we have

$$\frac{d\hat{\pi}^{(\kappa)}}{d\rho} = R_\kappa(\rho) \frac{d\pi}{du}. \quad (\text{C.3})$$

Substituting this into Eq. (C.1) and dividing by $R_\kappa(\rho) \neq 0$ yields a Riccati equation with constant coefficients,

$$\begin{aligned} \frac{d\hat{\pi}^{(\kappa)}}{du} &= -\frac{4}{3} (\hat{\pi}^{(\kappa)})^2 + \frac{10}{21} \hat{\pi}^{(\kappa)} + \frac{4}{3c}, \\ &= -\frac{4}{3} (\hat{\pi}^{(\kappa)} - \bar{\pi}_+)(\hat{\pi}^{(\kappa)} - \bar{\pi}_-), \end{aligned} \quad (\text{C.4})$$

where $\bar{\pi}_\pm$ are the fixed points of the Riccati differential equation (C.4)

$$\bar{\pi}_\pm = \frac{5}{28} \pm \frac{1}{28} \sqrt{25 + \frac{784}{c}}. \quad (\text{C.5})$$

Integrating Eq. (C.4) gives

$$\frac{1}{\bar{\pi}_+ - \bar{\pi}_-} \ln \left(\frac{\hat{\pi}^{(\kappa)} - \bar{\pi}_+}{\hat{\pi}^{(\kappa)} - \bar{\pi}_-} \right) = -\frac{4}{3} u + \bar{\pi}_0, \quad (\text{C.6})$$

with integration constant $\bar{\pi}_0$ determined by the initial condition $\hat{\pi}^{(\kappa)}(\rho_0)$. Solving for $\hat{\pi}^{(\kappa)}(u)$ and using $u = \ln S(\rho)$, we obtain the explicit solution for arbitrary $S_\kappa(\rho)$

$$\bar{\pi}_\kappa^{\text{cold}}(\rho) = \frac{\bar{\pi}_+ - \bar{\pi}_0 \bar{\pi}_- S_\kappa(\rho)^{-\frac{4}{3}(\bar{\pi}_+ - \bar{\pi}_-)}}{1 - \bar{\pi}_0 S_\kappa(\rho)^{-\frac{4}{3}(\bar{\pi}_+ - \bar{\pi}_-)}}. \quad (\text{C.7})$$

The analytic structure of the cold-limit solution (C.7) is that of a fractional linear (Möbius) map.

In Ref. [41], the authors identified the cold-limit solution of the traditional Israel–Stewart equation for the effective shear in the case of Gubser flow. Equation (C.1) reproduces their setup upon neglecting the term proportional to $10/21$ and using $S_\kappa(\rho) = \cosh \rho$. Solving the analogous IS equation for an arbitrary foliation - again dropping the $10/21$ term and following the same procedure outlined above - one finds that the cold-limit IS solution for a general $dS_3 \times \mathbb{R}$ slicing takes the form

$$\bar{\pi}_\kappa^{\text{IS-cold}} = \frac{1}{\sqrt{c}} \tanh \left(\frac{4}{3\sqrt{c}} [\ln S_\kappa(\rho) - \bar{\pi}_0 c] \right). \quad (\text{C.8})$$

Notice that the full second-order equation (C.1) cannot be reduced to the IS form by any deformation.

References

- [1] M. Krook and T.T. Wu, *Formation of maxwellian tails*, *Phys. Rev. Lett.* **36** (1976) 1107.
- [2] M. Krook and T.T. Wu, *Exact solutions of the boltzmann equation*, *Physics of Fluids* **20** (1977) 1589.
- [3] A.V. Bobylev, *Some properties of boltzmann's equation for maxwell molecules*, *Sov. Phys. Dokl.* **5/6** (1984).

- [4] G.S. Denicol, U.W. Heinz, M. Martinez, J. Noronha and M. Strickland, *New Exact Solution of the Relativistic Boltzmann Equation and its Hydrodynamic Limit*, *Phys. Rev. Lett.* **113** (2014) 202301 [[1408.5646](#)].
- [5] G.S. Denicol, U.W. Heinz, M. Martinez, J. Noronha and M. Strickland, *Studying the validity of relativistic hydrodynamics with a new exact solution of the Boltzmann equation*, *Phys. Rev. D* **90** (2014) 125026 [[1408.7048](#)].
- [6] D. Bazow, G.S. Denicol, U. Heinz, M. Martinez and J. Noronha, *Analytic solution of the Boltzmann equation in an expanding system*, *Phys. Rev. Lett.* **116** (2016) 022301 [[1507.07834](#)].
- [7] D. Bazow, G.S. Denicol, U. Heinz, M. Martinez and J. Noronha, *Nonlinear dynamics from the relativistic Boltzmann equation in the Friedmann-Lemaître-Robertson-Walker spacetime*, *Phys. Rev. D* **94** (2016) 125006 [[1607.05245](#)].
- [8] Y. Wang, X. Zhao, Z. Xu and J. Hu, *Analytical Solution and Lie Algebra of the Relativistic Boltzmann Equation*, [2511.08652](#).
- [9] Y. Hatta, M. Martinez and B.-W. Xiao, *Analytic solutions of the relativistic Boltzmann equation*, *Phys. Rev. D* **91** (2015) 085024 [[1502.05894](#)].
- [10] J. Noronha and G.S. Denicol, *Perfect fluidity of a dissipative system: Analytical solution for the Boltzmann equation in $\text{AdS}_2 \otimes \text{S}_2$* , *Phys. Rev. D* **92** (2015) 114032 [[1502.05892](#)].
- [11] J. Hu, *Analytical solution of the nonlinear relativistic Boltzmann equation*, *JHEP* **2025** (2025) 066 [[2411.16448](#)].
- [12] S. Chen and S. Shi, *Exact solution of Boltzmann equation in a longitudinal expanding system*, *Phys. Rev. C* **109** (2024) L051901 [[2311.09575](#)].
- [13] G. Baym, *Thermal Equilibration in Ultrarelativistic Heavy Ion Collisions*, *Phys. Lett. B* **138** (1984) 18.
- [14] SMASH collaboration, *Equilibration and freeze-out of an expanding gas in a transport approach in a Friedmann–Robertson–Walker metric*, *Phys. Lett. B* **770** (2017) 532 [[1612.06436](#)].
- [15] S.S. Gubser and A. Yarom, *Conformal hydrodynamics in Minkowski and de Sitter spacetimes*, *Nucl. Phys. B* **846** (2011) 469 [[1012.1314](#)].
- [16] J.D. Bjorken, *Highly Relativistic Nucleus-Nucleus Collisions: The Central Rapidity Region*, *Phys. Rev. D* **27** (1983) 140.
- [17] S.S. Gubser, *Symmetry constraints on generalizations of Bjorken flow*, *Phys. Rev. D* **82** (2010) 085027 [[1006.0006](#)].
- [18] S. Grozdanov, *A family of three maximally symmetric boost-invariant flows in relativistic hydrodynamics*, [2510.10769](#).
- [19] P. Rioseco and O. Sarbach, *Accretion of a relativistic, collisionless kinetic gas into a Schwarzschild black hole*, *Class. Quant. Grav.* **34** (2017) 095007 [[1611.02389](#)].
- [20] P. Rioseco, *Relativistic Kinetic Theory with Applications in Astrophysics*, Ph.D. thesis, PhD thesis, Universidad Michoacana de San Nicolás de Hidalgo, 2019.
- [21] R.O. Acuña-Cárdenas, C. Gabarrete and O. Sarbach, *An introduction to the relativistic kinetic theory on curved spacetimes*, *Gen. Rel. Grav.* **54** (2022) 23 [[2106.09235](#)].
- [22] O. Sarbach and T. Zannias, *Relativistic Kinetic Theory: An Introduction*, *AIP Conf. Proc.* **1548** (2013) 134 [[1303.2899](#)].

- [23] O. Sarbach and T. Zannias, *Tangent bundle formulation of a charged gas*, *AIP Conf. Proc.* **1577** (2015) 192 [[1311.3532](#)].
- [24] O. Sarbach and T. Zannias, *The geometry of the tangent bundle and the relativistic kinetic theory of gases*, *Class. Quant. Grav.* **31** (2014) 085013 [[1309.2036](#)].
- [25] S.R. de Groot, W.A. van Leeuwen and C.G. van Weert, *Relativistic Kinetic Theory: principles and applications*, Elsevier North-Holland (1980).
- [26] C. Cercignani and G. Medeiros Kremer, *The relativistic Boltzmann Equation: Theory and Applications*, Birkhäuser Verlag (Basel, Switzerland) (2002).
- [27] F. Debbasch and W. van Leeuwen, *General relativistic Boltzmann equation, I: Covariant treatment*, *Physica A: Statistical Mechanics and its Applications* **388** (2009) 1079.
- [28] F. Debbasch and W. van Leeuwen, *General relativistic Boltzmann equation, II: Manifestly covariant treatment*, *Physica A: Statistical Mechanics and its Applications* **388** (2009) 1818.
- [29] P.L. Bhatnagar, E.P. Gross and M. Krook, *A Model for Collision Processes in Gases. I. Small Amplitude Processes in Charged and Neutral One-Component Systems*, *Physical Review* **94** (1954) 511.
- [30] J. Anderson and H. Witting, *A relativistic relaxation-time model for the Boltzmann equation*, *Physica* **74** (1974) 466 .
- [31] G.S. Denicol, J. Noronha, H. Niemi and D.H. Rischke, *Origin of the Relaxation Time in Dissipative Fluid Dynamics*, *Phys. Rev. D* **83** (2011) 074019 [[1102.4780](#)].
- [32] W. Florkowski, R. Ryblewski and M. Strickland, *Testing viscous and anisotropic hydrodynamics in an exactly solvable case*, *Phys. Rev. C* **88** (2013) 024903 [[1305.7234](#)].
- [33] W. Florkowski, R. Ryblewski and M. Strickland, *Anisotropic Hydrodynamics for Rapidly Expanding Systems*, *Nucl. Phys. A* **916** (2013) 249 [[1304.0665](#)].
- [34] E. Beltrametti and A. Blasi, *On the number of Casimir operators associated with any Lie group*, *Physics Letters* **20** (1966) 62.
- [35] J.E. Humphreys, *Introduction to Lie algebras and representation theory*, vol. 9, Springer Science & Business Media (2012).
- [36] M. Martinez, M. McNelis and U. Heinz, *Anisotropic fluid dynamics for Gubser flow*, *Phys. Rev. C* **95** (2017) 054907 [[1703.10955](#)].
- [37] M. Martinez and C. Plumberg, *In preparation*, 2025.
- [38] B. Banerjee, R.S. Bhalerao and V. Ravishankar, *Equilibration of the Quark - Gluon Plasma Produced in Relativistic Heavy Ion Collisions*, *Phys. Lett. B* **224** (1989) 16.
- [39] I. Muller, *Zum Paradoxon der Wärmeleitungstheorie*, *Z. Phys.* **198** (1967) 329.
- [40] W. Israel and J.M. Stewart, *Transient relativistic thermodynamics and kinetic theory*, *Annals Phys.* **118** (1979) 341.
- [41] H. Marrochio, J. Noronha, G.S. Denicol, M. Luzum, S. Jeon and C. Gale, *Solutions of Conformal Israel-Stewart Relativistic Viscous Fluid Dynamics*, *Phys. Rev. C* **91** (2015) 014903 [[1307.6130](#)].
- [42] A. Soloviev, *Close encounters with attractors of the third kind*, [2510.26599](#).
- [43] J.F. Carinena and A. Ramos, *Integrability of Riccati equation from a group theoretical viewpoint*, *Int. J. Mod. Phys. A* **14** (1999) 1935 [[math-ph/9810005](#)].

- [44] V.V. Kisil, *Geometry of Möbius transformations: Elliptic, parabolic and hyperbolic actions of $SL_2(\mathbb{R})$* , World Scientific (2012).
- [45] F.S. Bemfica, M.M. Disconzi and J. Noronha, *Causality and existence of solutions of relativistic viscous fluid dynamics with gravity*, *Phys. Rev. D* **98** (2018) 104064 [[1708.06255](#)].
- [46] R. Baier, P. Romatschke, D.T. Son, A.O. Starinets and M.A. Stephanov, *Relativistic viscous hydrodynamics, conformal invariance, and holography*, *JHEP* **04** (2008) 100 [[0712.2451](#)].
- [47] U.W. Heinz and M. Martinez, *Investigating the domain of validity of the Gubser solution to the Boltzmann equation*, *Nucl. Phys. A* **943** (2015) 26 [[1506.07500](#)].
- [48] M.P. Do Carmo, *Riemannian Geometry*, Birkhäuser, Boston (1992).
- [49] J. Lee, *Introduction to Riemannian manifolds*, Springer (2018).